ISTITUTO NAZIONALE DI FISICA NUCLEARE

Sezione di Genova

INFN/BE-82/1
16 Giugno 1982

E. Di Salvo and G. A. Viano: SURFACE WAVES IN α-NUCLEI ELASTIC SCATTERING.

Servizio Documentazione
dei Laboratori Nazionali di Frascati

Istituto Nazionale di Fisica Nucleare
Sezione di Genova

INFN/BE-82/1
16 Giugno 1982

SURFACE WAVES IN α-NUCLEI ELASTIC SCATTERING

E. Di Salvo and G. A. Viano
INFN - Sezione di Genova, and Istituto di Scienze Fisiche dell'Università di Genova

ABSTRACT

We develop in detail a theory of surface waves, excited by the grazing rays in the elastic scattering of α particles on nuclei, working within the framework of the short wavelength approximation. The nuclear interaction region is schematized as an absorbing sphere surrounded by a nearly transparent shell; the surface waves, which are excited at the edge of the interaction region and propagate along it, can take one or more shortcuts. In this way we can explain the large angle elastic scattering of α particles on ^{16}O, ^{28}Si and ^{40}Ca from $\sim$20 to $\sim$60 MeV. Indeed the theory is tested by fitting the differential cross sections of these scattering processes. The nuclear interaction radii can be extracted from our phenomenological analysis.

1. - INTRODUCTION

In the geometrical theory of diffraction in the sense of Keller[1, 2], in addition to the classical optical rays (i. e. reflected, refracted etc.) also the 'diffracted rays' are introduced. In the light scattering these rays are produced by incident rays which are tangent to the surface of the body. If we assume that the body has a smooth surface and is opaque such that all the refracted rays are absorbed, then each tangent ray splits at the point of tangency. One part continues along the path of the incident ray; another part travels along the surface of the body, as a surface ray, describing a geodesic on the body surface. At each point it splits again, one part continuing along the surface and the other part leaving the surface along the tangent. Thus a single grazing incident ray produces infinitely many diffracted rays[1]. Introducing the diffracted rays, the classical geometrical optics is so modified as to include diffraction, and the ray tracing technique, which is very useful in practice, can be considerably extended accounting for the appearence of light in shadows.

Classically a way for relating the ray and wave formalism goes through the Malus theorem on normal congruences. A normal congruence is a family of rays, all of which are normal to some surface; such a surface is called a wavefront. The theorem of Malus guarantes that the rays, going through an optical system, retain the property of being normal to a family of surfaces; this theorem is applicable also to curved rays in non-uniform media. Moreover it holds also for diffracted rays and gives the possibility of describing the physics of the grazing rays using the wavefront formulation(1). Thus one can associate to the surface rays the surface waves which propagate along the surface of the body penetrating into the shadow region.

Since classical mechanics corresponds to the geometrical optics limit of a wave motion, in which the light rays orthogonal to the wavefronts correspond to the particle trajectories, it seems worth trying an extension of Keller's geometrical diffraction theory in the domain of mechanics. In this way one can use the ray tracing methods also for treating the diffraction in the scattering of particles and nuclei. Indeed the backward peaks in the elastic scattering cross-sections, which have been observed in α-nuclei, pion-proton and heavy-ion collisions, can be explained as due to surface waves which, propagating along the surface of the target and penetrating into the shadow, emerge at backwards.

In this paper we start from a Schrödinger equation for a complex valued cutoff potential; then we do a short wavelength approximation and obtain the eikonal and transport equations. Next, working with these equations, we analyse, with the ray tracing technique, the trajectories described by a beam of particles hitting a target. The main purpose is to develop a theory of surface waves generated by the grazing trajectories. Therefore we shall use concepts and words typical of optics, like diffraction, reflection, refraction, caustic and so on, referring to particle trajectories rather than to light rays. Then, starting from the surface wave theory, we can explain the enhancement of the differential cross-sections at large angles; moreover we take into account also possible phenomena of interference, e. g. with the reflected rays. Finally the theory, developed in Section 2, is tested in Section 3 trying to fit the differential cross-sections of the α-nuclei elastic scattering at backwards.

Now we must mention the anomalous large angle scattering (ALAS), which has been observed in α-nuclei and heavy ion collisions. In this paper we shall consider only the α-nuclei elastic scattering; then ALAS is particularly evident in the $^{40}Ca(\alpha,\alpha)^{40}Ca$ case, for an energy of the colliding α particles which ranges roughly from 25 to 50 MeV. Observing that 20 is a magic number and that the phenomenon attenuates for the isotopes of ^{40}Ca whose shells are open, it is quite natural to speak of an isotope effect of ALAS, which is probably related to the closed shell structure of the target.

A lot of papers have been devoted to the problem of the semiclassical scattering of α particles on nuclei (see e. g. Refs. (3,4) and references quoted therein). Furthermore various models have been proposed up to now for explaining ALAS, nor can we be exhaustive recalling each of them. Therefore we limit ourselves to illustrate with a few words the main ones, i. e. the rotator and the optical potential models.

A) Rotator model. - Since ALAS can be associated with the dominance of a packet of partial waves, whose angular momenta have a distribution centred on the grazing angular momentum, then one can try to fit the data with the introduction of a pole in the complex angular momentum plane. The pole, indeed, can be used as a classical mathematical tool for picturing a resonance produced, in this case, by a rotator (quasi-molecular rotator). Then ALAS can be seen as the envelope of resonances produced by the rotations of colliding particles around the target, or as a rotational band of resonances, to which it corresponds a straight line pole trajectory[5, 6]. This model is somewhat reminiscent of the "orbiting" in the sense of Ford-Wheeler[7].

B) Optical model potential. - It is generally assumed that the α-nucleus scattering can be described by a complex potential; all the inelastic channels are taken into account in bulk by the imaginary part of the potential. In most analyses the form of the potential chosen is generally of the Woods-Saxon type. In recent years, when more precise data have been available, other forms seem to be superior[8]. Then many modifications have been proposed like to take a Woods-Saxon squared form factor[8] or an angular momentum dependent absorption[9, 10], etc. Within the optical potential framework some semiclassical models have been proposed. One of these, due to Brink et al.[11], explains ALAS as due to the dominance of the "internal waves", i. e. the waves which pass inside the external potential barrier and reemerge; then the interference between the internal and the barrier reflected waves can explain the shape of the differential cross-sections.

The mechanism of the surface waves was firstly invoked, as far as we know, by Bryant and Jarmie[12] for explaining the backward peaks in α-nuclei elastic scattering. This model is similar to that of the rotator and in both cases one makes use of poles of the S-function in the complex angular momentum plane. Some authors[13] identify the rotational resonances with the surface waves in the α-^{40}Ca system. However we must recall that, if one considers the high frequency light scattering by a transparent sphere[14], then one finds two different classes of poles in the complex angular momentum plane. The poles of the first class are located near the real axis and are associated with the single particle resonances; they are, indeed, connected with the "interior" of the potential. The poles of the second class lie along a line which is nearly parallel to the imaginary axis; they are insensitive to the behaviour of the potential in the inner region and are associated with surface waves. Furthermore these second class poles move approximately parallel to the real axis with increasing energy(14). The distinction between these two classes of poles is probably less neat if one introduces a complex valued potential (i. e. absorption); nevertheless, owing to the above exposed arguments, we prefer to retain the distinction between resonances and surface waves. In fact the phenomenological analysis, which shall be made in Section 3, shows that the poles, which we find, behave like surface wave poles, since they move approximately parallel to the real axis with increasing energy.

Now let us examine our model in some detail. We schematize the nuclear interaction region in a way which differs somewhat from the picture usually adopted. Indeed we think that the target cannot be schematized simply as a black sphere. Then we shall work with a complex-valued potential whose imaginary part has a radius smaller than the real one. In other words we suppose that there is a transparent shell at the periphery of the interaction region. Then the grazing rays may describe simply an arc of geodesic around the target or also, being critically refracted, take one or more shortcuts before emerging tangentially at the surface. The mechanism of the shortcut is necessary in order to explain the anomalously large backward peaks in the elastic scattering cross-sections; otherwise the exponential damping along the surface is too large to allow a strong enhancement at large angles. The existence of shortcuts is strictly related to the opaqueness of the target; this latter is determined by the number of open channels. Since this number is smallest for ^{40}Ca and largest for ^{44}Ca(10), the isotope effect can be explained admitting the existence of shortcuts for closed shell nuclei and their attenuation, for a larger opaqueness, when one considers the isotopes. Analogously the opaqueness increases toward larger energies, and this could explain the fact that the anomalous backward peaks tend to become normal for greater values of the energy.

We shall derive the theory of the surface waves working with a cutoff potential. This choice, which can appear unsatisfactory, is due to the fact that this theory is quite complex and, for the moment, it appears very hard to extend it to more realistic continuous potentials. However we shall use the potential only as a suitable laboratory for deriving a set of formulae which describe the core of the surface wave model; then the goodness of the model is tested by fitting the experimental data with these formulae. So doing our procedure differs considerably from the standard one. In this latter one firstly fits the experimental cross-sections in order to determine a potential; then the mechanism of the physical model is analyzed and checked on the potential itself. However this method is not free from defects. Indeed it is impossible to avoid many types of ambiguities in the potential determination. In fact regarding this problem as the inverse problem in the scattering theory, it can be shown that, even if the uniquesness of the solution can be proved, nevertheless the continuity in the dependence of the potential on the scattering data is lacking(15), in the sense that very small perturbations of the data (such as those produced by the experimental errors) can produce arbitrarily large instabilities in the potential, especially at the edge of the interaction region. Indeed the inverse problem in potential scattering is an example of those problems which have been classified as "improperly posed" by Hadamard(16). In conclusion, since our line of approach differs considerably from the standard one, a comparison between our model and those based on optical potentials cannot be made clearly.

Our paper is organized as follows : in Section 2 we develop the surface wave theory along the lines explained above ; Section 3 is devoted to the phenomenological analysis.

2. - SURFACE WAVE THEORY

2. 1. - Preliminaries

Let us start from the stationary Schrödinger equation, which can be written as follows :

$$\Delta\psi + k^2 n^2 \psi = 0 \tag{1}$$

where

$$n^2 = 1 - \frac{U(r)}{E} , \qquad k = \frac{(2\mu E)^{1/2}}{\hbar} \tag{2}$$

μ being the reduced mass. We assume a potential $U(r)$ of the following form :

$$U(r) = \begin{cases} V_c(r) + V_N(r) & r \leq R \quad (3a) \\ \dfrac{2\eta}{kr} E & r > R \quad (3b) \end{cases}$$

where η is the Sommerfeld parameter : $\eta = (\mu Z Z' e^2)/(\hbar^2 k)$. V_c is the electrostatic potential inside the nucleus. V_N, which describes the nuclear interaction, is complex-valued and reads as follows :

$$V_N(r) = - V_o - i\, W_o(r) \tag{4}$$

here V_o is a positive constant and $W_o(r)$ is some positive function which goes rapidly to zero as $r \to R$, in such a way that it leaves a nearly transparent shell at the periphery of the nuclear interaction region. Of course we cannot exclude that a particle, which travels at the periphery of the nuclear interaction regiion, has some probability of causing inelastic scattering. However, for the sake of simplicity, we shall regard the peripheral shell of the interaction sphere as if it were transparent. Finally we assume that $W_o(r)$ does not cause any appreciable reflection.

In the approximation of short wave-lengths, it is convenient to write the wavefunction as a linear superposition of terms like $A(\underline{r})\exp\left[i\Phi(\underline{r})\right]$, such that each one satisfies eq. (1).

Upon substituting in eq. (1) we get, for large values of k :

$$(\nabla\Phi)^2 = n^2 k^2 , \tag{5}$$

$$\nabla \cdot (A^2 \nabla\Phi) = 0 . \tag{6}$$

The eqs. (5) and (6) are respectively the eikonal and the transport equations. They hold true in regions where n(r) does not change greatly over distances of the order of the wave-length. This requirement is certainly not satisfied at the points of discontinuity of n, i. e. at r = R, where phenomena of reflection, refraction or diffraction occur.

In the following subsections we shall develop the eikonal method wherever possible. In subsections 2. 2 and 2. 3 we solve the eikonal equation, examining the various kinds of trajectories which can occur. In subsection 2. 4 we study the trasport equation and apply it to the different classes of trajectories. Then we describe the phenomena of diffraction (subsection 2. 5) and reflection subsection 3. 6), which are beyond a pure eikonal approximation. At this point we are able to write the wavefunction. From this we extract the scattering amplitude. Indeed we decompose, as usual, the wavefunction at large values of r, in terms of the incident and outgoing wave as follows :

$$\psi(k, r, \vartheta) \longrightarrow \psi_{inc}(k, r, \vartheta) + F(k, \vartheta)\, \frac{e^{i\left[kr - \eta \log 2kr\right]}}{r} , \tag{7}$$

where, following Nussenzveig[9], we set $F(k, \vartheta) = Rf(k, \vartheta)$, in such a way that $f(k, \vartheta)$ is a dimensionless quantity. Finally from the expression of the scattering amplitude $f(k, \vartheta)$ we derive the formula of the differential cross-section (subsection 2. 7).

2. 2. - The eikonal equation

The eikonal equation is identical in form with the Hamilton-Jacobi equation for Hamilton's characteristic function[17]. In polar coordinatesthis equation assumes the following form :

$$\left(\frac{\partial\Phi}{\partial r}\right)^2 + \frac{1}{r^2}\left(\frac{\partial\Phi}{\partial\vartheta}\right)^2 + \frac{1}{r^2 \sin^2\vartheta}\left(\frac{\partial\Phi}{\partial\varphi}\right)^2 = n^2 k^2 . \tag{8}$$

The variables in eq. (8) may be separated by assuming a solution of the form :

$$\Phi(r, \vartheta, \varphi) = \Phi_1(r) + \Phi_2(\vartheta) + \Phi_3(\varphi) . \tag{9}$$

Upon substituting this trial solution in eq. (8) we obtain:

$$\left(\frac{\partial \Phi_1}{\partial r}\right)^2 + \frac{\lambda^2}{r^2} = n^2 k^2 , \tag{10. a}$$

$$\left(\frac{\partial \Phi_2}{\partial \vartheta}\right)^2 + \frac{\lambda_\varphi^2}{\sin^2 \vartheta} = \lambda^2 , \tag{10. b}$$

$$\frac{\partial \Phi_3}{\partial \varphi} = \lambda_\varphi , \tag{10. c}$$

where λ is the magnitude of the total angular momentum and λ_φ that of its component along the polar axis. Here we take the origin of the coordinate system coincident with the centre of the nuclear interaction sphere, and the direction of the polar axis as being opposite to that of the incident beam; then $\lambda_\varphi = 0$. Next, integrating the eqs. (10), we get:

$$\Phi = \lambda\vartheta + \int r^{-1} (n^2 k^2 r^2 - \lambda^2)^{1/2} \, dr . \tag{11}$$

As prescribed by the Hamilton-Jacobi theory[17], the equation of the trajectory is given by

$$\frac{\partial \Phi}{\partial \lambda} = \vartheta_o , \tag{12}$$

where ϑ_o is the initial value of the polar coordinate ϑ. From eqs. (11) and (12) we have:

$$\vartheta = \vartheta_o + \int \frac{dr}{r(n^2 k^2 r^2 - \lambda^2)^{1/2}} . \tag{13}$$

If, along the trajectory, n(r) is continuous and slowly varying, then the trajectory is symmetric with respect to its apsidal point, as one can see from (13). If, on the contrary, the trajectory meets a point of discontinuity of n(r), reflection, refraction and possibly diffraction occur. Concerning the refracted and diffracted trajectories, they will be treated apart. The reflected trajectories are symmetric with respect to the point of reflection. Then, in the following, we shall denote by $\bar{r}$ indifferently the apsidal point or the reflection point of a trajectory.

Now we are interested to a tract of trajectory that begins at a distance r_o from the origin and ends at a distance r, after passing through $\bar{r}$. Subsequently the starting point and the end point of the trajectory shall be pushed to infinity. Therefore from eq. (11) we have:

$$\Phi = \lambda\vartheta + I + I_o , \tag{14. a}$$

where

$$I = I(\lambda, \bar{r}, r) = \int_{\bar{r}}^{r} \frac{(n^2 k^2 r'^2 - \lambda^2)^{1/2}}{r'} dr' \tag{14. b}$$

and

$$I_o = I(\lambda, \bar{r}, r_o) = \int_{\bar{r}}^{r_o} \frac{(n^2 k^2 r'^2 - \lambda^2)^{1/2}}{r'} dr' . \tag{14. c}$$

Then eq. (13) can be rewritten as follows:

$$\vartheta = \vartheta_o - \frac{\partial I}{\partial \lambda} - \frac{\partial I_o}{\partial \lambda} \tag{15}$$

Finally substituting eq. (15) in eq. (14. a), we get:

$$\Phi = \lambda (\vartheta_o - \frac{\partial I}{\partial \lambda} - \frac{\partial I_o}{\partial \lambda}) + I + I_o . \tag{16}$$

Now we consider the region $r > R$; here n^2 is given by $n^2 = 1 - \frac{2\eta}{kr}$. Then we integrate I obtaining

$$I(\lambda, \bar{r}, r) = \int_{\bar{r}}^{r} \frac{(k^2 r'^2 - 2\eta k r' - \lambda^2)^{1/2}}{r'} dr' = \Big[(k^2 r'^2 - 2\eta k r' - \lambda^2)^{1/2} - \eta \log \left| (k^2 r'^2 - 2\eta k r' - \lambda^2)^{1/2} + kr' - \eta \right| + \lambda \arcsin \frac{\eta k r' + \lambda^2}{kr'(\lambda^2 + \eta^2)^{1/2}} \Big]_{\bar{r}}^{r} . \tag{17}$$

For large values of r we get:

$$I = kr - \eta - \eta \log 2kr + \lambda \arcsin \frac{\eta}{(\lambda^2 + \eta^2)^{1/2}} - \lambda \arcsin \frac{\eta k\bar{r} + \lambda^2}{k\bar{r}(\lambda^2 + \eta^2)^{1/2}} - (k^2 \bar{r}^2 - 2\eta k\bar{r} - \lambda^2)^{1/2} + \eta \log \left| (k^2 \bar{r}^2 - 2\eta k \bar{r} - \lambda^2)^{1/2} + k\bar{r} - \eta \right| + O(r^{-1}). \tag{18}$$

Next deriving I with respect to λ we have:

$$\frac{\partial I}{\partial \lambda} = \arcsin \frac{\eta}{(\lambda^2 + \eta^2)^{1/2}} - \arcsin \frac{\eta k\bar{r} + \lambda^2}{k\bar{r}(\lambda^2 + \eta^2)^{1/2}} + O(r^{-1}) . \tag{19}$$

Note that, neglecting terms of order r^{-1}, $\partial I / \partial \lambda$ can be expressed as the difference between the following angles:

$$\bar{\vartheta}_c = \arcsin \frac{\eta}{(\lambda^2 + \eta^2)^{1/2}} \tag{20, a}$$

$$\bar{\vartheta}_i = \arcsin \frac{\eta k\bar{r} + \lambda^2}{k\bar{r}(\lambda^2 + \eta^2)^{1/2}} . \qquad (20.b)$$

Analogous expressions can be obtained for I_o and $\partial I_o/\partial\lambda$; it is sufficient to write r_o, in place of r, in eqs. (17), (18) and (19).

Now, when we make r_o tend to infinity, ϑ_o tends to zero. On the other hand, when also $r \to \infty$, ϑ becomes the deflection angle, which shall be denoted by Θ. Then, recalling eq. (15), we obtain for Θ the following expression:

$$\Theta = 2(\bar{\vartheta}_i - \bar{\vartheta}_c). \qquad (21)$$

Generally the scattering amplitude is written in terms of the scattering angle, i. e. the angle between the scattered and incident direction. This angle is the supplement of Θ, except for the diffracted rays, which shall be treated apart (see Appendix). In order to avoid notational proliferation, we shall denote, hereafter, the scattering angle with ϑ. Then, even if we use the same symbol for a polar coordinate and for the scattering angle, we shall see that, in practice, this does not lead to any sort of ambiguity.

In order to obtain the expression of Φ, we substitute the expressions of I and $\partial I/\partial\lambda$, given by formulae (18) and (19), and the analogous expressions of I_o and $\partial I_o/\partial\lambda$ in formula (16); moreover we subtract from Φ the phase of the incident wave[18], i. e.

$$\Phi_o = kr_o - \eta \log 2kr_o . \qquad (22)$$

In conclusion, denoting once more with Φ the phase, even after the subtraction, we get:

$$\Phi = 2\Delta + kr - \eta \log 2kr \qquad (23)$$

where

$$\Delta = \eta \left[\log \left| (k^2\bar{r}^2 - 2\eta k\bar{r} - \lambda^2)^{1/2} + k\bar{r} - \eta \right| - 1 \right] - (k^2\bar{r}^2 - 2\eta k\bar{r} - \lambda^2)^{1/2} . \qquad (24)$$

2. 3. - Trajectories.

In our problem it is useful to distinguish among various classes of trajectories. Let us consider, firstly, the trajectory of a particle of charge Z'e under the action of the sole Coulomb field of a point-like charge Ze; then it is straightforward to derive, in the framework of the Hamilton-Jacobi theory, the expression of its apsidal distance from the origin. We can compare this distance - which we denote by ϱ - with the radius R of the nuclear potential. Then $\varrho(\lambda)$ can be larger, equal or smaller than R. Accordingly we have three different classes of trajectories:

a) The trajectories, which correspond to those angular momenta such that $\varrho > R$, are determined by the action of the sole Coulomb field. In the following these trajectories shall be called "Coulomb trajectories", and all the quantities referring to this class of trajectories shall have the index c.

b) The trajectories, which correspond to $\varrho = R$, may be diffracted or critically refracted, they shall be called "grazing trajectories", and all the quantities referring to this class of trajectoris shall have the index g.

c) The trajectories, which correspond to those angular momenta such that $\varrho < R$, are reflected or refracted at the surface of the nuclear interaction sphere. The refracted trajectories are largerly absorbed by the opaque core of the target. Nevertheless we cannot exclude their contribution to the elastic cross-section. In particular, at backwards, they could even produce the geometrical glory peak. However for the values of kR that we are considering, this effect results to be negligible in comparison to the contribution of the surface waves[14]. Then, hereafter, we shall work with the following approximate scheme: only the critically refracted rays are transmitted through the transparent shell of the nuclear interaction sphere, while the refracted rays are absorbed by the opaque core of the interaction region. Furthermore we neglact the surface waves which are possibly excited at the edge of the opacity region. Therefore the trajectories belonging to this third class are only the "reflected trajectories", and all the quantities referring to this class of trajectories shall have the index r.

Now let us see in detail the analytical expressions of the deflection functions and of the phase-shift Δ for these different classes of trajectories.

a) For the trajectories belonging to the first class $\bar{r}$ coincides with ϱ. Since ϱ is given by:

$$\varrho = \frac{1}{k}\left[\eta + (\lambda^2 + \eta^2)^{1/2}\right] \tag{25}$$

then, from eqs. (20) and (21), we obtain for the deflection angle the following expression:

$$\Theta_c = \pi - 2\arcsin\frac{\eta}{(\lambda^2+\eta^2)^{1/2}} = \pi - 2\bar{\vartheta}_c \ . \tag{26}$$

For the scattering angle ϑ_c we get:

$$\vartheta_c = \pi - \Theta_c = 2\bar{\vartheta}_c \ . \tag{27}$$

Finally substituting in eq. (24), in place of $\bar{r}$, the expression (25) of ϱ, we have:

$$\Delta_c = \eta\left[\log(\lambda^2+\eta^2)^{1/2} - 1\right]. \tag{28}$$

Next, inverting eq. (27), we obtain:

$$\lambda = \eta \cot g \frac{\vartheta_c}{2} . \tag{29}$$

Substituting eq. (29) in eq. (28), we get:

$$\Delta_c = \eta \left[\log \frac{\eta}{\sin(\vartheta_c/2)} - 1 \right] . \tag{30}$$

In order to write the phase of the semiclassical Coulomb scattering amplitude, we must keep into account an additional phase difference of $-\pi/2$ between the incident and the outgoing wave due to the crossing of the trajectory through the turning point, which is a point of the caustic of the Coulomb trajectories. Therefore the phase of the Coulomb amplitude in our approximation is given by $2\Delta_c - \frac{\pi}{2}$. This result can be obtained also by a saddle point evaluation of the partial wave expansion of the Coulomb amplitude, provided that the Coulomb phase shift is approximated by[19]

$$\sigma(\lambda) = \lambda \arcsin \frac{\eta}{(\lambda^2 + \eta^2)^{1/2}} + \eta \left[\log(\lambda^2 + \eta^2)^{1/2} - 1 \right] . \tag{31}$$

This latter approximation holds true if $\eta \gg 1$.

b) We can obtain the deflection angle and the other quantities referring to the grazing trajectories, if we specify the value of λ in formulae (26), (27), (28), using the angular momentum of the grazing trajectory, i. e.

$$\lambda_g = kR\left(1 - \frac{2\eta}{kR}\right)^{1/2} = k_c R ; \qquad \left(k_c = k\left(1 - \frac{2\eta}{kR}\right)^{1/2}\right) . \tag{32}$$

Then from eq. (26) we obtain:

$$\Theta_g = \pi - 2 \arcsin \frac{\eta}{(kR - \eta)} . \tag{33}$$

From eq. (27) we have:

$$\vartheta_g = \pi - \Theta_g = 2 \arcsin \frac{\eta}{(kR - \eta)} \tag{34}$$

which represents the scattering angle of a grazing trajectory that does not undergo any diffraction or refraction. Finally from eq. (28) we obtain:

$$\Delta_g = \eta \left[\log(kR - \eta) - 1 \right] . \tag{35}$$

c) For the reflected trajectories $\bar{r}$ is given by the radius R, and $\lambda < \lambda_g$. Then the deflection angle Θ_r is given by formula (21) where $\bar{\vartheta}_i$ reads as follows:

$$\bar{\vartheta}_i = \arcsin \frac{\eta k R + \lambda^2}{kR(\lambda^2 + \eta^2)^{1/2}} \tag{36}$$

and $\bar{\vartheta}_c$ is given by formula (20. a). The scattering angle $\vartheta_r = \pi - \Theta_r$ is related to $\bar{\vartheta}_i$ and $\bar{\vartheta}_c$ as follows:

$$\cos \frac{\vartheta_r}{2} = \sin(\bar{\vartheta}_i - \bar{\vartheta}_c). \tag{37}$$

Finally writing R in place of $\bar{r}$ in formula (24) we obtain:

$$\Delta_r = \eta \left\{ \log \left[(\lambda_g^2 - \lambda^2)^{1/2} + kR - \eta \right] - 1 \right\} - (\lambda_g^2 - \lambda^2)^{1/2}. \tag{38}$$

We conclude this subsection observing that in the angular region $\vartheta > \vartheta_g$, we do not have the contribution of "Coulomb trajectories", whereas the contribution of reflected trajectories must be taken into account. On the other hand the diffracted rays contribute at every angle. Moreover there is a transition region around ϑ_g, where we cannot employ the eikonal approximation, due to the strong interference among incident, reflected and diffracted rays.

2. 4. - The transport equation.

Let us consider a wavefront Σ_o and a finite portion σ_o of Σ_o; denote by V the volume swept by σ_o as it becomes σ. We apply the divergence theorem to eq. (6) obtaining:

$$\int_V \nabla \cdot (A^2 \nabla \Phi) \, dV = \int_S A^2 \nabla \Phi \cdot \underline{dS} = 0 \tag{39}$$

where $S = \partial V$ (i. e. it is the boundary of V). It is straightforward to derive from eq. (39):

$$\int_{\sigma_o} A^2 \nabla \Phi \cdot \underline{d\sigma_o} = \int_{\sigma} A^2 \nabla \Phi \cdot \underline{d\sigma} \, . \tag{40}$$

Next, using the eikonal eq. (5), we can rewrite eq. (40) in the following form:

$$\int_{\sigma_o} A^2 n \, d\sigma_o = \int_{\sigma} A^2 n \, d\sigma \, . \tag{41}$$

Now we introduce a parametric representation for the surfaces σ_o and σ by means of the vectors :

$$\underline{r}^o = \underline{r}^o(u, v) \quad , \tag{42.a}$$

$$\underline{r} = \underline{r}(U, V) \quad . \tag{42.b}$$

Moreover setting $B = A^2 n$ we can rewrite once more eq. (41) as follows :

$$\int_{\tau_o} B(r^o) \left| \underline{r}_u^o \times \underline{r}_v^o \right| du\, dv = \int_{\tau} B(r) \left| \underline{r}_U \times \underline{r}_V \right| dU\, dV \tag{43}$$

where $\left| \underline{r}_u^o \times \underline{r}_v^o \right|$ and $\left| \underline{r}_U \times \underline{r}_V \right|$ are the moduli of the so-called fundamental vector products, $\underline{r}_u^o$ being the derivative of the vector $\underline{r}^o$ with respect to u (analogously for $\underline{r}_v^o$, $\underline{r}_U$, $\underline{r}_V$).

Finally if we change the variables in the right-hand side of formula (43) as follows : $U = U(u, v)$, $V = V(u, v)$, then the transformation formula for double integrals states that :

$$\int_{\tau} B(\underline{r}) \left| \underline{r}_U \times \underline{r}_V \right| dU\, dV = \int_{\tau_o} B(\underline{r}) \left| \underline{r}_U \times \underline{r}_V \right| \left| \frac{\partial(U, V)}{\partial(u, v)} \right| du\, dv \; . \tag{44}$$

Comparing the left-hand side of eq. (43) with the right-hand side of formula (44) and observing that that this equality does not depend on the particular tube of trajectories which has been chosen, we derive the following equality :

$$B(\underline{r}^o) \left| \underline{r}_u^o \times \underline{r}_v^o \right| = B(\underline{r}) \left| \underline{r}_U \times \underline{r}_V \right| \left| \frac{\partial(U, V)}{\partial(u, v)} \right| . \tag{45}$$

Before going to apply eq. (45) to the classes of trajectories that we have considered above, let us do some considerations on the incident beam.

The wavefront of the incident beam, at large distance from the nuclear interaction region, is not properly a plane, and this is due to the long range of the Coulomb field. The equation of this wavefront, for large values of r_o, can be written in terms of polar coordinates (r_o, ϑ_o) as follows[18]

$$k r_o \cos \vartheta_o + \eta \log \left[k r_o (1 + \cos \vartheta_o) \right] = \text{const} \quad . \tag{46}$$

However it is preferable to write the vector $\underline{r}^o$ as a function of the impact parameter b and of the azimuth angle φ. Indeed from eq. (46) it follows :

$$\left| \underline{r}_b^o \times r_\varphi^o \right| = b(1 + O(r_o^{-4})) \; . \tag{47}$$

Now we go to consider separately the different classes of trajectories.

a) The wavefront of the trajectories belonging to the first class ("Coulomb trajectories"), at large distance from the nuclear interaction region, is spherical. Then it can be properly described by the spherical coordinates ϑ, φ. The modulus of the fundamental vector product is given by (see formula (A. 2)):

$$\left| \underline{r}_{\vartheta} \times \underline{r}_{\varphi} \right| = r^2 \sin \vartheta_c (1 + O(r^{-2})) \tag{48}$$

where ϑ_c is, indeed, the scattering angle of the Coulomb trajectories. Then applying eq. (45) and taking into account only the main term for large values of r we obtain:

$$A_c(r, \vartheta_c) = \frac{A_o}{r} \left(\frac{b}{\sin \vartheta_c}\right)^{1/2} \left| \frac{d\vartheta_c}{db} \right|^{-1/2}, \tag{49}$$

where A_o is the amplitude of the incident beam, which we set equal to 1 owing to the normalization constraint. Finally evaluating $\left| d\vartheta_c / db \right|$ through eq. (27) we obtain:

$$A_c(r, \vartheta_c) = \frac{1}{2kR} \frac{\eta}{\sin^2(\vartheta_c/2)} . \tag{50}$$

b) As far as the grazing rays are concerned, the transport equation can be employed in some separate sections of the path. In particular, this equation can be applied to the incident rays up to the point of incidence, then to the critically refracted rays and, lastly, to the diffracted rays as they leave the surface of the sphere. In the last case, however, we must keep in mind that the surface is a caustic of the diffracted rays. All these applications of the transport equation are studied in the Appendix, where the grazing ray contribution is deduced in detail.

c) As regards the reflected rays we use twice eq. (45), comparing firstly the amplitude of the incident beam with that near the interaction region; then the reflected amplitude near the sphere is compared with the one scattered at large distance. The final result is given by

$$A_r(r, \vartheta_r) = \frac{1}{r} \left(\frac{b}{\sin \vartheta_r}\right)^{1/2} \left| \frac{d\vartheta_r}{db} \right|^{-1/2} \mathscr{R}(\vartheta_r), \tag{51}$$

where the factor $\mathscr{R}(\vartheta_r)$ is the reflection coefficient and the term $\left| d\vartheta_r/db \right|$ can be evaluated through eq. (37). Both of them shall be reconsidered below in subsection 2. 6.

2. 5. - Surface waves.

In this subsection we shall start with the ray tracing of the diffracted rays, following closely the method of Chen[20] and Nussenzveig[14]. We consider all the grazing rays which emerge in a direction ϑ, after taking $0, 1, 2, \ldots, p$ shortcuts inside the transparent shell of the nuclear interaction sphere. For a general value of p, a ray, before emerging in a direction ϑ, has to describe arcs of amplitude φ_j such that:

$$\sum_j \varphi_j = \zeta^{\pm}_{p,m} = \zeta^{\pm}_{p} + 2m\pi, \qquad m = 0, 1, 2, \ldots \tag{52. a}$$

where

$$\zeta^{\pm}_{p} = \pm \vartheta + \vartheta_g - p\vartheta_t\,(\mathrm{mod}(2\pi)), \qquad (0 \leq \zeta^{\pm}_{p} \leq 2\pi), \tag{52. b}$$

ϑ_t being the amplitude of the arc corresponding to the shortcut. We denote by $\zeta^{+}_{p,m}$ the arc described by the counterlockwise travelling surface wave, while $\zeta^{-}_{p,m}$ is the arc described by the clockwise travelling one.

We must consider p different kinds of rays, according as they have $0, 1, \ldots, p-1$ internal reflections. In this connection it is useful to distinguish between two types of vertices: we denominate type (i) vertices those at which an internal reflection takes place, type (ii) vertices those at which two critical refractions occur. In the simplest case the ray describes an arc φ, then it has $p-1$ internal reflections (i.e. $p-1$ type (i) vertices) and lastly describes an arc $(\zeta^{\pm}_{p,m} - \varphi)$. Another class of rays can be obtained by substituting one type (i) by one type (ii) vertex. Similarly all the possible classes of rays are obtained by substituting $2, 3, \ldots$ type (i) vertices by $2, 3, \ldots$ type (ii) vertices. Next we make a simplifying assumption: we neglect the rays for which $m \geqslant 1$.

Now the reader is referred to the Appendix where we have derived the contribution of the diffracted rays to the wave function in two cases: $p = 0$ and $p = 1$, assuming that the rays propagate in the counterlockwise direction. From the wave-function we can derive the scattering amplitude. The formulae which we obtain can be read regarding the coefficients D, D', D_{12}, D_{21} as coupling constants characterizing tha various types of interactions, and the terms $\exp(i\,\lambda\,\zeta^{\pm}_{p})$, $\exp(i\,\Phi_s)$ as propagators. More precisely any point at which diffraction, critical refraction or internal reflection takes place may be regarded as an interaction vertex, and a proper coupling constant may be defined for any type of interaction. They are:

a) the diffraction coefficients D and D';

b) D_{12} and D_{21} for the rays which have a critical refraction entering into or emerging from the sphere;

c) R_{22} for the internal reflection.

Moreover the line joining two vertices may be regarded as a propagator. We must distinguish between two cases, and precisely:

a) For a surface ray describing an arc of amplitude $\zeta_p^{\pm}$ the propagator takes the form $\exp\left[i\,\lambda\,\zeta_p^{\pm}\right]$, where

$$\lambda = k_c R + i\alpha \,, \tag{53}$$

α being the decay exponent of the surface wave.

b) The propagator for a shortcut can be easily deduced from the Hamilton-Jacobi theory outlined above, and it is given by

$$e^{i\Phi_s} = e^{i\left[\lambda_g \vartheta_t + 2\int_{\bar{r}}^{R} (n^2 k^2 - \lambda_g^2 r^{-2})^{1/2}\, dr\right]} \tag{54}$$

where

$$n^2 = 1 - \frac{V_c(r) - V_o}{E} \tag{55}$$

and $\bar{r}$ is the minimal distance from the centre of the sphere.

The coupling constant and the propagators depend on the local properties of the surface and on k_c (2, 20). This is in agreement with so-called "localization principle" (14) which ensures us that, in the limit of short wavelenghts, the phenomena that occur at the periphery of the interaction region are essentially independent of the inner structure.

Now looking at formulae (A. 26) and (A. 30) we see that, apart some factors like $\exp\left\{2i\eta\left[\log(kR - \eta) - 1\right]\right\}$ or $(\cos\frac{\vartheta_g}{2})^{-1/2}$ which depend on the Coulomb field, there remains the term $(\sin\vartheta)^{-1/2}$, which requires some comments. In fact the diffracted rays form an axial caustic, which is the straight line parallel to the incident beam, passing through the centre of the interaction sphere. Here the ray approximation does not hold; however the focusing effect due to the caustic in the backward direction is described by the factor $(\sin\vartheta)^{-1/2}$.

It is convenient to write the scattering amplitude produced by the diffracted rays (it shall be denoted hereafter by $f_d(k,\vartheta)$), as the sum of different contributions $f_d^{(p)}(k,\vartheta)$, corresponding to the various values of p. Furthermore each term $f_d^{(p)}(k,\vartheta)$ is to be further decomposed into the contributions of the counterlockwise and clockwise rays as follows:

$$f_d(k,\vartheta) = \sum_p f_d^{(p)}(k,\vartheta) = \sum_p \left[f_d^{(p)^+}(k,\vartheta) + f_d^{(p)^-}(k,\vartheta)\right] \tag{56}$$

In fact we must take into account a phase shift of $-\pi/2$ between $f_d^{(p)^-}(k,\vartheta)$ and $f_d^{(p)^+}(k,\vartheta)$, since the clockwise rays cross the focal points once more than the counterclockwise ones. Therefore in the expressions of $f_d^{(p)^+}$ and $f_d^{(p)^-}$ we shall introduce two phase factors $i^{n_p^+}$ and $i^{n_p^-}$ respectively, such that: $n_p^- = n_p^+ - 1$.

At this point we have at our disposal all the rules which allow us to write explicitly the scattering amplitudes $f_d^{(p)\pm}(k,\vartheta)$. Let us consider, for instance, the case $p=0$. The surface waves are excited at T_1 and T_2 and are reconverted at S_1 and S_2 into tangentially emerging rays (see Fig. 1). Then applying the rules, that we have exposed above, one can directly write the scattering amplitudes as follows :

$$f_d^{(o)+}(k,\vartheta) = \frac{-iDe^{i\lambda(\vartheta+\vartheta_g)}}{(\sin\vartheta)^{1/2}} \frac{D'}{(\cos\vartheta_g/2)^{1/2}} e^{2i\Delta_g} , \tag{57. a}$$

$$f_d^{(o)-}(k,\vartheta) = -\frac{De^{i\lambda(2\pi-\vartheta+\vartheta_g)}}{(\sin\vartheta)^{1/2}} \frac{D'}{(\cos\vartheta_g/2)^{1/2}} e^{2i\Delta_g} . \tag{57. b}$$

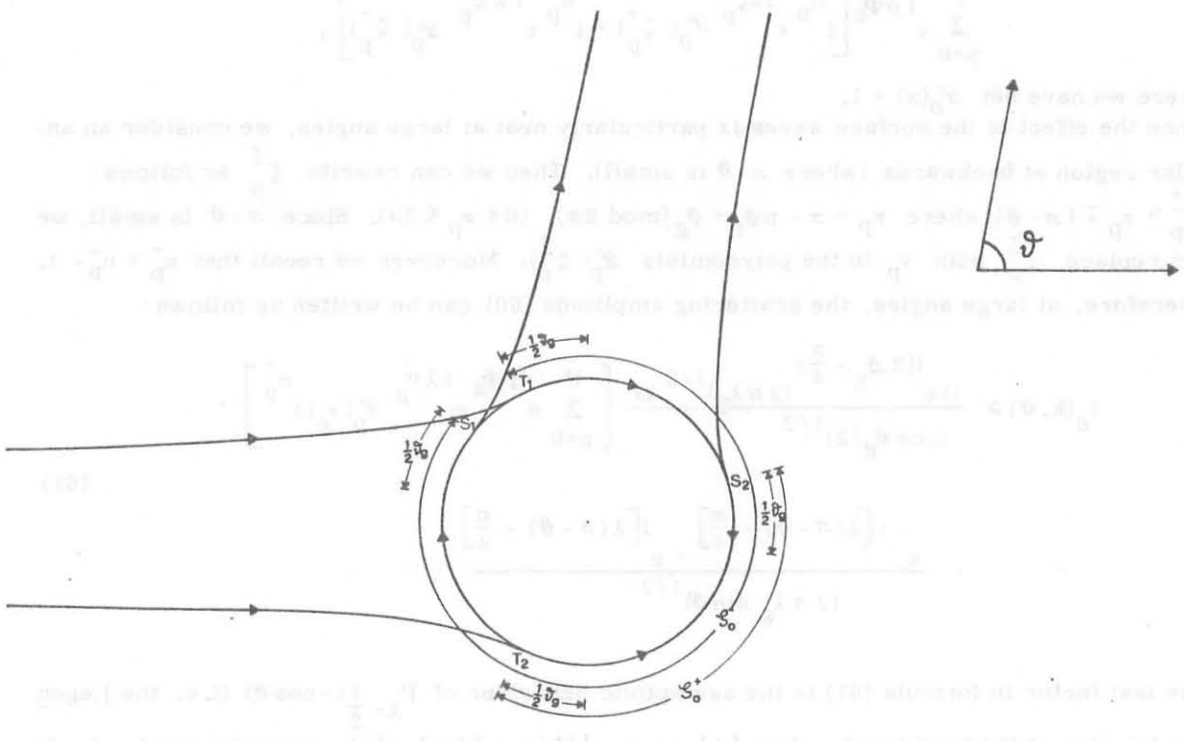

FIG. 1 - Diffracted rays in the direction ϑ : case $p=0$.

For the p-th term ($p \geqslant 1$) we have (see also refs. (14, 21)):

$$f_d^{(p)\pm}(k,\vartheta) = \frac{i^{n_p^\pm} De^{ip\Phi_s} e^{i\lambda\zeta_p^\pm}}{(\sin\vartheta)^{1/2}} \frac{D'}{(\cos\vartheta_g/2)^{1/2}} e^{2i\Delta_g} \cdot \sum_{m=1}^{p} \binom{p-1}{m-1} (R_{22})^{(p-m)} (D_{12}D_{21})^m \frac{(\zeta_p^\pm)^m}{m!} . \tag{58}$$

Hereafter, in order to shorten our formulas, we introduce the following polynomials:

$$\mathscr{L}_p(\zeta_p^{\pm}) = \sum_{m=1}^{p} \binom{p-1}{m-1} (R_{22})^{(p-m)} (D_{12} D_{21})^m \frac{(\zeta_p^{\pm})^m}{m!} \qquad (p \geq 1) \tag{59}$$

The next step is to substitute formulas (58), (59) in formula (56). As Nussenzveig[14] has shown, the sum (56) is to be truncated after P terms, where P is of the order of $(k_c R)^{2/3}$. Then we obtain:

$$f_d(k,\vartheta) \simeq \sum_{p=0}^{P} \left[f_d^{(p)^+}(k,\vartheta) + f_d^{(p)^-}(k,\vartheta) \right] = \frac{D e^{2i\Delta_g} D'}{(\sin\vartheta)^{1/2} (\cos\vartheta_g/2)^{1/2}} \cdot$$

$$\cdot \sum_{p=0}^{P} e^{ip\Phi_s} \left[i^{n_p^+} e^{i\lambda\zeta_p^+} \mathscr{L}_p(\zeta_p^+) + i^{n_p^-} e^{i\lambda\zeta_p^-} \mathscr{L}_p(\zeta_p^-) \right], \tag{60}$$

where we have set $\mathscr{L}_o(x) = 1$.

Since the effect of the surface waves is particularly neat at large angles, we consider an angular region at backwards (where $\pi - \vartheta$ is small). Then we can rewrite $\zeta_p^{\pm}$ as follows: $\zeta_p^{\pm} = \nu_p \mp (\pi - \vartheta)$ where $\nu_p = \pi - p\vartheta_t + \vartheta_g \,(\mathrm{mod}\ 2\pi)$, $(0 \leq \nu_p \leq 2\pi)$. Since $\pi - \vartheta$ is small, we can replace $\zeta_p^{\pm}$ with ν_p in the polynomials $\mathscr{L}_p(\zeta_p^{\pm})$. Moreover we recall that $n_p^- = n_p^+ - 1$. Therefore, at large angles, the scattering amplitude (60) can be written as follows:

$$f_d(k,\vartheta) \simeq \frac{D e^{i(2\Delta_g - \frac{\pi}{4})} (2\pi\lambda_g)^{1/2} D'}{(\cos\vartheta_g/2)^{1/2}} \left[\sum_{p=0}^{P} e^{ip\Phi_s} e^{i\lambda\nu_p} \mathscr{L}_p(\nu_p) i^{n_p^+} \right] \cdot$$

$$\cdot \frac{e^{-i\left[\lambda(\pi-\vartheta) - \frac{\pi}{4}\right]} + e^{i\left[\lambda(\pi-\vartheta) - \frac{\pi}{4}\right]}}{(2\pi\lambda_g \sin\vartheta)^{1/2}} . \tag{61}$$

The last factor in formula (61) is the asymptotic behaviour of $P_{\lambda - \frac{1}{2}}(-\cos\vartheta)$ (i.e. the Legendre function of the first kind), when $|\lambda| \to \infty$. $|\lambda|(\pi - \vartheta) \gg 1$ (λ is approximated by λ_g in the denominator). Then writing the Legendre function instead of its asymptotic behaviour we have:

$$f_d(k,\vartheta) \simeq \frac{D e^{i(2\Delta_g - \frac{\pi}{4})} (2\pi\lambda_g)^{1/2} D'}{(\cos\vartheta_g/2)^{1/2}} \cdot$$

$$\cdot \left[\sum_{p=0}^{P} e^{ip\Phi_s} e^{i\lambda\nu_p} \mathscr{L}_p(\nu_p) i^{n_p^+} \right] P_{\lambda - \frac{1}{2}}(-\cos\vartheta) \tag{62}$$

which gives the correct contribution of the surface waves even in a neighbourhood of the axial caustic (see also Levy-Keller[(2)]).

2. 6. - The reflected rays.

Now we go to consider the reflected ray contribution. In the wavefunction this will be of the form $A_r(r, \vartheta_r)\exp\left[i\Phi_r(r, \vartheta_r)\right]$, where $\Phi_r(r, \vartheta_r)$ reads as follows (see formula (23)):

$$\Phi_r(r, \vartheta_r) = 2\Delta_r + kR - \eta\log 2kR \tag{63}$$

and Δ_r is given by eq. (38). The amplitude A_r can be deduced from eq. (51). Indeed, using eq. (37), we can evaluate the term $\left(\frac{b}{\sin\vartheta_r}\right)^{1/2}\left|\frac{d\vartheta_r}{db}\right|^{-1/2}$. Recalling that $\lambda = kb$, we get:

$$\left(\frac{b}{\sin\vartheta_r}\right)^{1/2}\left|\frac{d\vartheta_r}{db}\right|^{-1/2} = \frac{R}{2}\left[\mathscr{F}(\vartheta_r)\right]^{-1/2} \tag{64}$$

where

$$\mathscr{F}(\vartheta_r) = \frac{(\cos\vartheta_r/2)^2}{\gamma^2} + \cos\left(\frac{\vartheta_r}{2}\right)\frac{2(\gamma - \cos(\vartheta_r/2)) + \gamma\delta(1 - 2\delta - \gamma^2)^{-1/2}}{\gamma^2 + \delta^2} \tag{65}$$

$$\left(\gamma = \frac{\lambda}{kR}\,;\quad \delta = \frac{\eta}{kR}\right)$$

Writing the contribution to the wavefunction of the reflected rays, and comparing this with the asymptotic expression of the wavefunction (formula (7)) we extract the scattering amplitude for the reflected rays:

$$f_r(k, \vartheta_r) = \frac{1}{2}\left[\mathscr{F}(\vartheta_r)\right]^{-1/2} e^{2i\Delta_r}\,\mathscr{R}(\vartheta_r)\,. \tag{66}$$

As far as $\mathscr{R}(\vartheta_r)$ is concerned, we use the Fresnel reflection coefficient, i.e. we make the approximation of considering the reflection as that produced by a plane wave on a plane interface:

$$\mathscr{R}(\vartheta_r) = -\frac{K_r - k_r}{K_r + k_r}\,, \tag{67}$$

where

$$K_r = (k_r^2 + 2\mu\hbar^{-2}V_o)^{1/2} \tag{68}$$

and

$$k_r = \left[k^2\left(1 - \frac{2\eta}{kR}\right) - \frac{\lambda^2}{R^2}\right]^{1/2}. \tag{69}$$

In formula (67) (as well as in formula (63)) the dependence on ϑ_r can be made explicit through the function $\lambda(\vartheta_r)$, which can be obtained inverting eq. (37).

2. 7. - Differential cross-sections.

Summing the contribution of the surface waves to that of the reflected rays (which now can be written omitting the index r in the notation of the angle ϑ_r), we obtain a cross-section of the following form :

$$\left(\frac{d\sigma}{d\Omega}\right) = R^2 \left| f(k,\vartheta) \right|^2 = R^2 \left| A\, e^{i\chi} P_{\lambda-\frac{1}{2}}(-\cos\vartheta) + \frac{1}{2}\, e^{2i\Delta_r} \mathscr{R}(\vartheta) \left[\mathscr{F}(\vartheta)\right]^{-1/2} \right|^2 \tag{70}$$

where A and χ are real valued functions such that

$$A\, e^{i\chi} = \frac{D(2\pi\lambda_g)^{1/2}\, e^{i(2\Delta_g - \frac{\pi}{4})}}{(\cos\vartheta_g/2)^{1/2}}\, D' \left[\sum_{p=0}^{P} e^{ip\Phi_s}\, e^{i\lambda\nu_p} \mathscr{L}_p(\nu_p)\, i^{n_p^+} \right]. \tag{71}$$

We recall that the reflection amplitude, which appears in formula (70), has been deduced assuming a sharp edge for the nuclear interaction region. But in the next section we shall see that this assumption is too drastic for fitting the experimental data. Indeed we shall be obliged to modify the reflection amplitude following a more realistic hypothesis of a diffuse edge. In this case the reflection amplitude becomes negligible as the energy increases, and the cross-section reduces to the surface wave contribution alone. This latter, at a fixed energy, reads as follows :

$$\frac{d\sigma}{d\Omega} \simeq C \left| P_{\lambda-\frac{1}{2}}(-\cos\vartheta) \right|^2 \tag{72}$$

where $C = R^2 A^2$. On the other hand, at fixed angle ($\vartheta = 180^o$), we have $P_{\lambda-\frac{1}{2}}(-\cos\vartheta) = 1$, and then from (70), (71) we get :

$$\left(\frac{d\sigma}{d\Omega}\right)_{\vartheta=\pi} = \frac{2\pi\lambda_g R^2}{\cos(\vartheta_g/2)} \left| D D' \sum_{p=0}^{P} e^{ip\Phi_s} \mathscr{L}_p(\nu_p)\, e^{i(\lambda\nu_p + \frac{\pi}{2} n_p^+)} \right|^2 . \tag{73}$$

3. - PHENOMENOLOGICAL ANALYSIS.

In this Section we present and comment the fits of the experimental data. We have focused our attention on three examples : $^{16}O(\alpha,\alpha)^{16}O$, $^{28}Si(\alpha,\alpha)^{28}Si$, $^{40}Ca(\alpha,\alpha)^{40}Ca$. Since in the latter case we have been able to find a larger number of experimental data, especially at higher energies, the analysis is more complete and richer.

One can try two different types of fits :

a) at fixed energy,

b) at fixed angle.

Considering the first class of fits, let us do some preliminary observations. Firstly, we fit the data in a restricted angular region near 180°, which coincides roughly with the region where the glory effect, produced by the surface waves, is dominant, i. e. $\pi - \vartheta \lesssim (k_c R)^{-1/2}$ (see ref. (14)). However, as we shall see, in some cases we can extend our fits to a larger angular region. Moreover, as is clearly shown in the figures which are given below, it is evident the necessity of separating the fits at energies larger than ~ 35 MeV. from the ones at energies which range between 22 and 35 MeV.

In Figgs. 2, 3 the backward elastic scattering cross-sections of α particles from ^{40}Ca are fitted by formula (72), where C and $Re\lambda$, $Im\lambda$ are regarded as free parameters; the energy range considered is from 36 to 62 MeV. The fits shown in these figures extend as far as the agreement with the data is satisfactory; then we see that in the energy range from 36 MeV to ~ 50 MeV our fit generally works up to $\vartheta \simeq 135^{\circ}$ (Fig. 2), whereas in the range from ~ 50 MeV to 62 MeV we can generally extend our fit up to $\vartheta \simeq 110^{\circ}$; below we shall give a tentative explanation of this fact. $Re\lambda$ and $Im\lambda$ are reported in Table I. In Fig. 4 we report analogous fits for the scattering $^{16}O(\alpha, \alpha)^{16}O$, in the energy range from 37 to 50 MeV; $Re\lambda$ and $Im\lambda$ are reported in Table III. In this case the experimental data are less abundant, then the fits, shown in the figure, stop at different angles, since we use all the data which we have at our disposal at various energies.

As shown in Figs. 2, 3, 4, the agreement of the fits to the data is good enough to say that the sole effect of the surface waves is sufficient to explain the backward peaks and oscillations. Then returning to the variation with the energy of the angular region where the fit works (variation which has been observed in the $^{40}Ca(\alpha, \alpha)^{40}Ca$ case), we can tentatively advance the following explanation. This variation can be correlated to the decrease of the backward peak, which starts at ~ 36 MeV, but becomes significant for energies larger than 50 MeV. This might be due to the fact that at higher energies new inelastic and reaction channels open; this causes an expansion of the absorptive region and consequently an attenuation of the amplitude of the surface rays that undergo one or more shortcuts : the larger the number of p (i. e. of shortcuts), the stronger the attenuation. Now, in these fits at fixed energy that we are considering, we use formula (72), which holds true as long as we can neglect the angular dependence in the polynomials $\mathscr{L}_p(\zeta_p^{\pm})$. This approximation is acceptable in an angular region sufficiently near 180°; for larger angular regions the exact cross-section deviates considerably from formula (72), since the angular dependence of the terms $\mathscr{L}_p(\zeta_p^{\pm})$ can no longer be neglected. This dependence is more accentuated for large values of p, while it is more bland for lower p. Since,

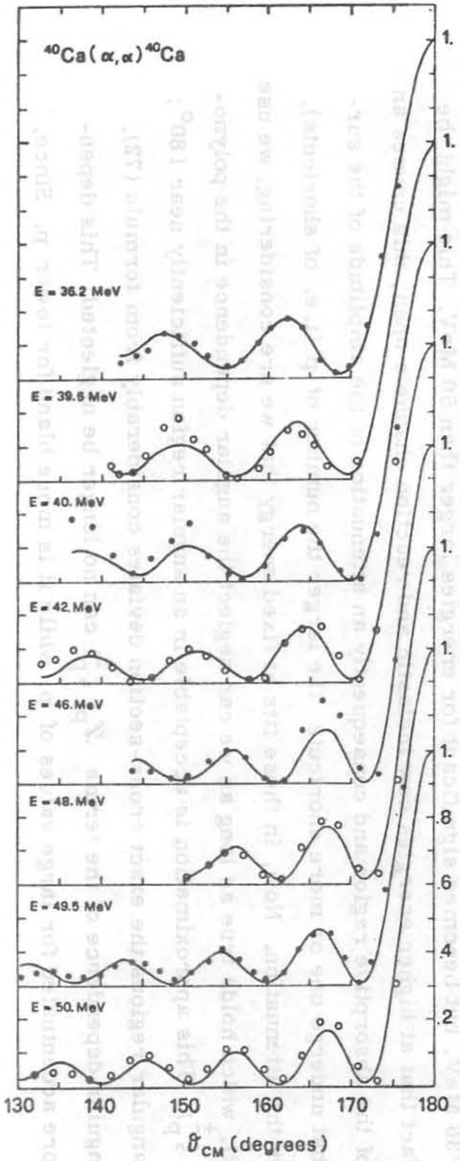

FIG. 2 - Fits to $^{40}Ca(\alpha, \alpha)^{40}Ca$ data from 36.2 to 50 MeV. The sets at E= = 36.2, 39.6 and 49.5 MeV have been taken from ref. (22), while the remaining ones have been taken from ref. (23).

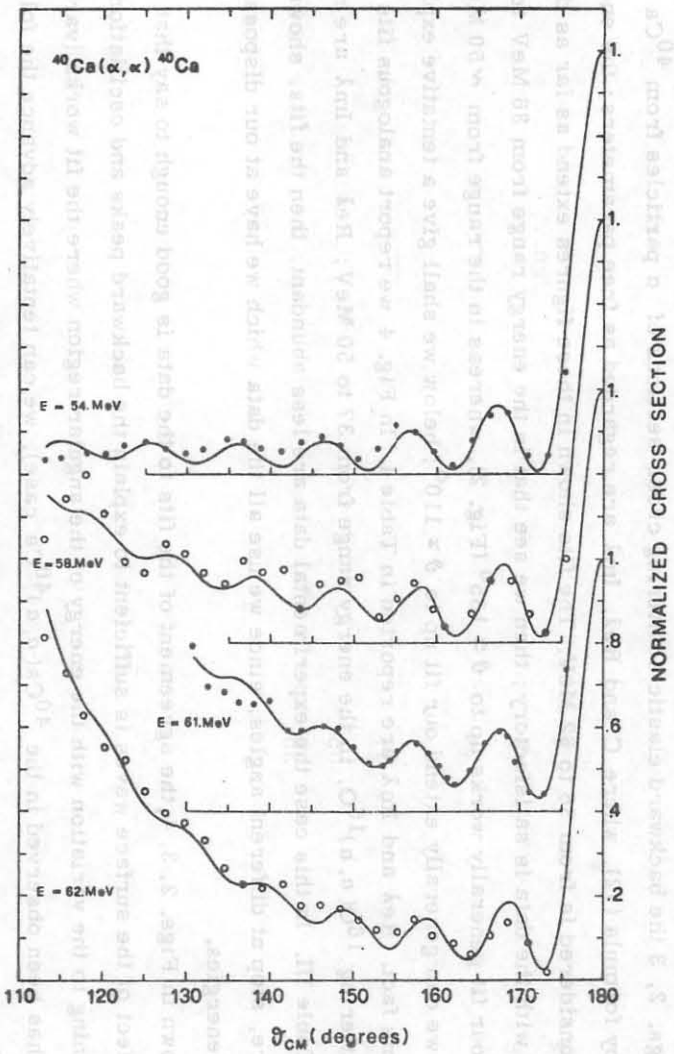

FIG. 3 - Fits to $^{40}Ca(\alpha, \alpha)^{40}Ca$ data from 54 to 62 MeV. The set at E = 61 MeV is taken from ref. (22), the other three from ref. (23).

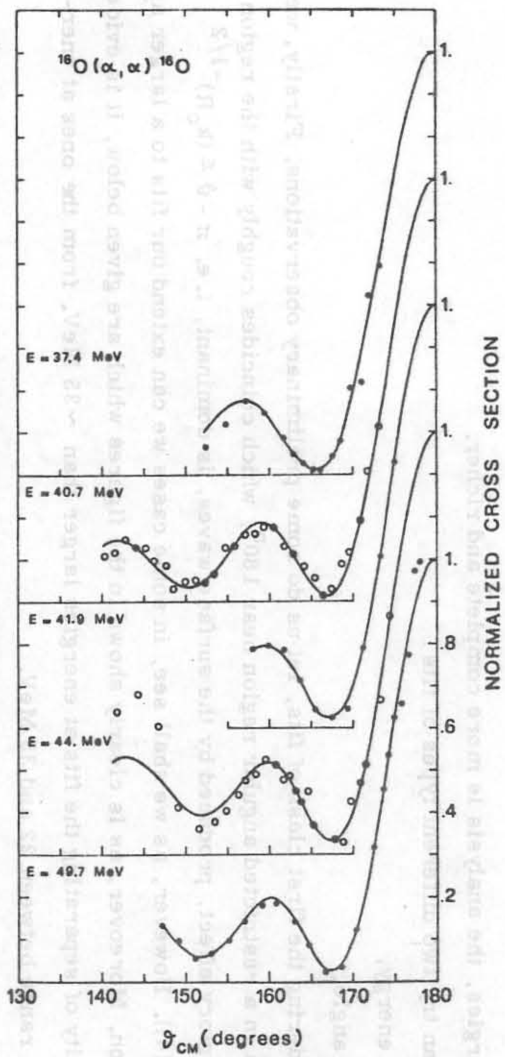

FIG. 4 - Fits to $^{16}O(\alpha, \alpha)^{16}O$ data from 37.4 to 49.7 MeV. The sets at E = 41.9 and 49.7 MeV have been taken from ref. (24), the other three from ref. (25).

TABLE I

Values of the parameters Reλ and Imλ, as obtained in the fits to the $^{40}Ca(\alpha,\alpha)^{40}Ca$ data at fixed energies : column a refers to the fits where only the surface ray contribution is considered; column b refers to the fits where the interference between surface rays is taken into account.

E_{lab} (MeV)	Reλ		Imλ	
	a	b	a	b
23. 4	10. 4	10. 3	0. 70	0. 70
24. 1	10. 4	10. 5	0. 71	0. 85
24. 7	10. 7	10. 8	0. 91	1. 00
25. 2	10. 4	10. 1	0. 99	0. 83
26. 4	10. 6	10. 1	0. 73	0. 62
36. 2	12. 5		1. 04	
39. 6	13. 3		0. 78	
40.	13. 9		0. 83	
42.	14. 2		0. 61	
46.	16. 5		0. 41	
48	17.		1. 05	
49. 5	15. 8		0. 55	
50.	17. 1		0. 70	
54.	17. 4		0. 78	
58.	18. 3		1. 57	
61.	17. 8		2. 04	
62.	19.		1. 95	

TABLE II

Values of the parameters Reλ and Imλ, as obtained in the fits to the $^{28}Si(\alpha,\alpha)^{28}Si$ data at fixed energies. See the legend of Table I.

E_{lab} (MeV)	Reλ		Imλ	
	a	b	a	b
22. 7	7. 6	7. 6	0. 88	1. 11
25. 2	10. 5	10. 6	1. 02	1. 06
27. 5	11. 1	11. 5	0. 80	1. 01
30. 0	13. 4	12. 9	2. 80	2. 34

TABLE III

Values of the parameters Reλ and Imλ, as obtained in the $^{16}O(\alpha,\alpha)^{16}O$ data at fixed energies.

E_{lab} (MeV)	Reλ	Imλ
25. 4	8. 0	0. 51
26. 6	8. 3	0. 96
29. 1	9. 4	0. 20
30. 0	9. 2	0. 20
30. 9	9. 9	0. 23
32. 2	10. 2	0. 30
37. 4	9. 6	0. 67
40. 7	10. 7	1. 01
41. 9	11. 0	1. 27
44. 0	11. 1	1. 58
49. 7	11. 3	1. 31

at higher energies, the amplitudes corresponding to the larger values of p are attenuated, our approximate formula (72) can be extended to a larger angular range.

Now if we try to fit, with fromula (72), the cross-section of $^{40}Ca(\alpha,\alpha)^{40}Ca$, at backwards, in the energy range from 23 to ~ 35 MeV, the agreement is unsatisfactory as shown in Fig. 5a. We find an analogous situation in the case $^{28}Si(\alpha,\alpha)^{28}Si$, as shown in Fig. 6a, where we report the fits in the energy from 22 to 30 MeV and only one fit is good. Therefore

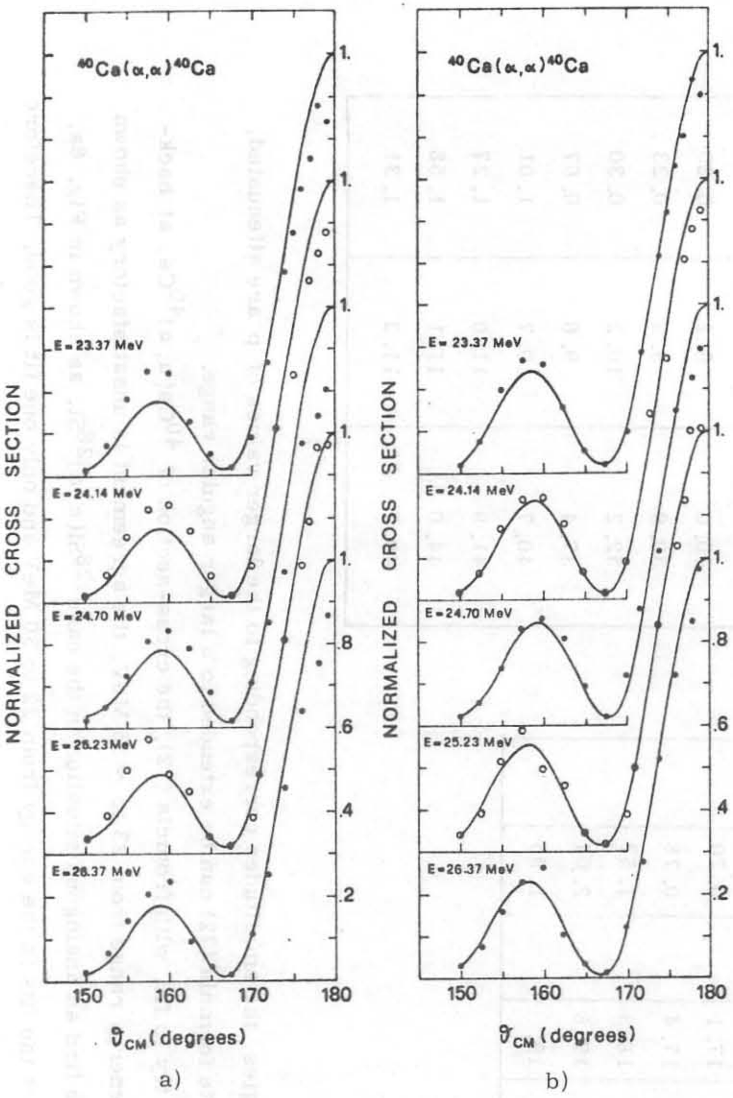

FIG. 5 - Fits to $^{40}Ca(\alpha,\alpha)^{40}Ca$ data from 23.37 to 26.37 MeV: a) the fits are made considering only the surface ray contribution; b) the interference with the reflected rays is taken into account. The data are taken from ref. (26).

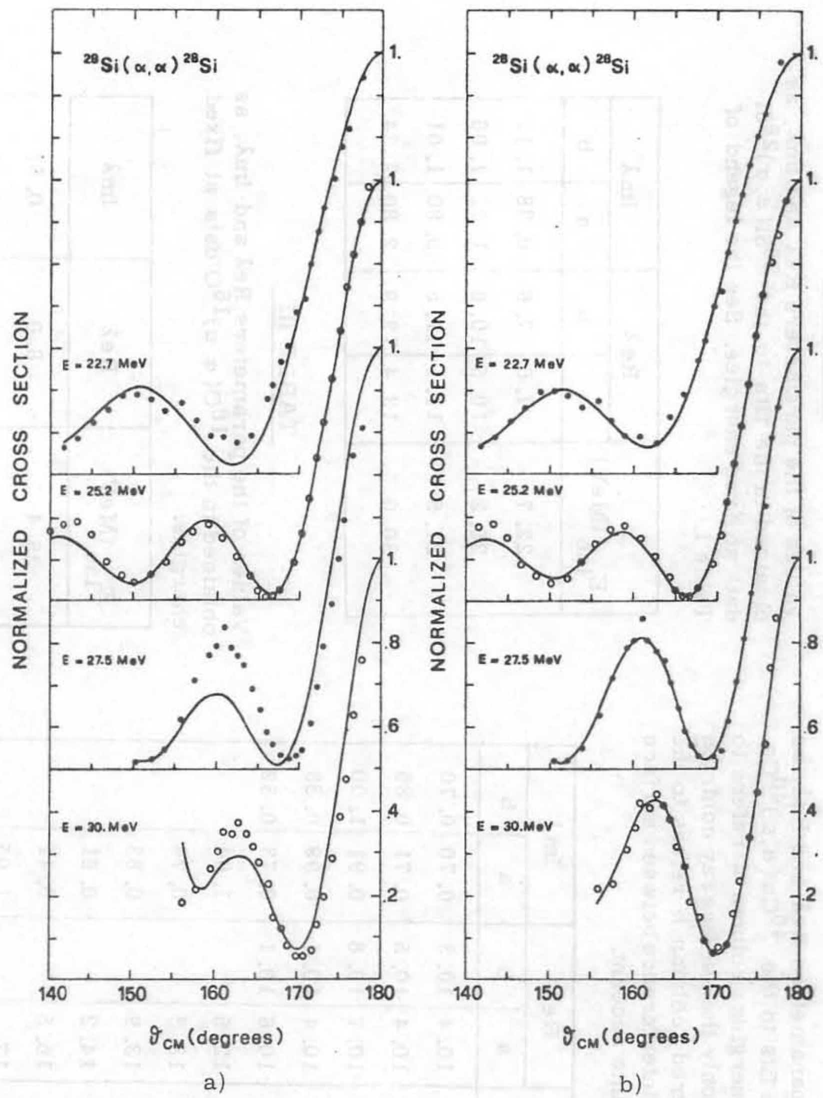

FIG. 6 - Fits to $^{28}Si(\alpha,\alpha)^{28}Si$ data from 22.7 to 30 MeV: a) the fits are made considering only the surface ray contribution; b) the interference with the reflected rays is taken into account. The data are taken from ref. (27).

we think that it is worth trying to fit the data taking into account the interference between the surface rays and the reflected rays. Accordingly we should fit the data with formula (70); however this fit is not successful. This, perhaps, can be explained noting that a cutoff potential is a too drastic approximation for evaluating correctly the reflected rays. Therefore we modify formula (70) adopting for the real part of the nuclear potential a Woods-Saxon shape instead of a square well, i. e.

$$V(r) = - V_o \left\{ 1 + \exp\left[(r - R_{V_o}) / \Delta_{V_o} \right] \right\}^{-1} , \tag{74}$$

where R_{V_o} and Δ_{V_o} are respectively the radius and the diffuseness. Accordingly formula (66) will be modified as follows:

$$f_r^{\mu}(k, \vartheta_r) = \frac{1}{2} \left[\mathscr{F}^{\mu}(\vartheta_r) \right]^{-1/2} e^{2i\Delta_r^{\mu}} \mathscr{R}^{\mu}(\vartheta_r) \tag{75}$$

where Δ_r^{μ} and $\mathscr{F}^{\mu}(\vartheta_r)$ are given by formulae (38) and (65) respectively, but using R_{V_o} instead of R: $\mathscr{R}^{\mu}(\vartheta_r)$ is given by

$$\mathscr{R}^{\mu}(\vartheta_r) = \frac{\Gamma(2i\Delta_{V_o}k_r)\Gamma(-i\Delta_{V_o}\left[K_r + k_r\right])\Gamma(1 - i\Delta_{V_o}\left[K_r + k_r\right])}{\Gamma(-2i\Delta_{V_o}k_r)\Gamma(-i\Delta_{V_o}\left[K_r - k_r\right])\Gamma(1 - i\Delta_{V_o}\left[K_r - k_r\right])} \tag{76}$$

where Γ is the Euler gamma function, while K_r and k_r are given by formulae (68) and (69) respectively, where now R_{V_o} is used in place of R. The reflection coefficient $\mathscr{R}^{\mu}(\vartheta_r)$ for a spherical Woods-Saxon potential has been obtained following a procedure proposed by Anni et al.[19]. This procedure consists in modifying the reflection coefficient of the one dimensional Woods-Saxon barrier[18], taking in place of the incident momentum its radial component. In formula (75) we have neglected the distortion caused by the Woods-Saxon shape of the potential on the trajectories of the incident particles; this approximation seems to be acceptable, due to the short range of the nuclear interaction. Lastly we observe that formula (76) reduces to formula (67) for $\Delta_{V_o} \to 0$.

Concerning the first term appearing in formula (70), we can reasonably assume that it needs not to be modified. Indeed, due to the small value of diffuseness that we find in fitting the data, V(r) varies very rapidly near the edge of the interaction region. Consequently it is not out of place to speak still of surface waves and of shortcuts. In conclusion we use the following formula:

$$\left(\frac{d\sigma}{d\Omega}\right) = R_{V_o}^2 \left| A e^{i\chi} P_{\lambda - \frac{1}{2}}(-\cos\vartheta) + f_r^{\mu}(k, \vartheta) \right|^2 , \tag{77}$$

where $f_r(k, \vartheta)$ is given by formula (75), while $A \exp(i\chi)$ is defined by formula (71). Here we use A, χ, $\mathrm{Re}\lambda$, $\mathrm{Im}\lambda$ as free parameters. Concerning V_o and R_{V_o}, we use the values obtained by Michel et al.[8] in the case of $^{40}Ca(\alpha,\alpha)^{40}Ca$ and by Lega et al.[32] in the case of $^{28}Si(\alpha,\alpha)^{28}Si$. These values of V_o and R_{V_o} are taken fixed in fitting the various sets of data at different energies. On the other hand the diffuseness obtained by these authors is too large to fit suitably the experimental data. Therefore we leave Δ_{V_o} free, but still independent of energy. We obtain for Δ_{V_o} the same value for $^{40}Ca(\alpha,\alpha)^{40}Ca$ and for $^{28}Si(\alpha,\alpha)^{28}Si$ scattering; it is given by $\Delta_{V_o} = 0.28 \pm 0.01$ fm.

The fits that we obtain for $^{40}Ca(\alpha,\alpha)^{40}Ca$ scattering are shown in Fig. 5b; the fits relative to $^{28}Si(\alpha,\alpha)^{28}Si$ scattering are presented in Fig. 6b. The values obtained for $\mathrm{Re}\lambda$ and $\mathrm{Im}\lambda$ are reported in Tables I and II respectively and they do not change significantly with respect to the values obtained neglecting the reflected rays. The agreement of the fits to the data is satisfactory. More precisely, let us take the ratio χ^2/(degrees of freedom) both for the fits in which only the surface waves are considered and for the fits in which the interference is taken into account: we find that in the latter case the ratio is always considerably lower than in the former case. Finally let us observe that in all these cases the fits stop at $\vartheta \simeq 150^o$, nor can they be extended further. This feature can, perhaps, be related to the fact that for $E \lesssim 35$ MeV the contribution of the surface waves with higher values of p (i. e. surface waves which take two or more shortcuts) cannot be neglected. This implies that our approximation works only in an angular region at backwards, where the glory effect is strictly dominant and the angular dependence in the polynomials $\mathcal{L}_p(\zeta_p^{\pm})$ can be neglected.

The analysis of the $^{16}O(\alpha,\alpha)^{16}O$ scattering looks quite different. Indeed we succeed in obtaining good fits, even in the energy region from 22 to 32 MeV, considering the sole effect of the surface waves, but the values that we obtain for $\mathrm{Im}\lambda$ are surprisingly small. This anomaly has been already remarked by Cowley and Heymann[28]. The fits are shown in Fig. 7 and $\mathrm{Re}\lambda$, $\mathrm{Im}\lambda$ are reported in Table III. Let us observe, however, that for $\mathrm{Im}\lambda$ we get values which are larger that those of ref. (28): this is obtained restricting the angular region of the fits at backwards where, as we have already remarked, the glory effect is strictly dominant.

Before going to the analysis of the values of λ which have been obtained in the fits, let us spend a few words of comments about the dependence of λ on k. In this connection we observe that α (see formula (53)) represents a quantum corrective term with respect to λ_g: then $\alpha/\lambda_g \to 0$ as $k \to \infty$. Therefore it is reasonable to approximate $\mathrm{Re}\lambda$ by λ_g, i. e. to fit the values of $\mathrm{Re}\lambda$, that we have found in the fits, using formula (32).

The fits to $\mathrm{Re}\lambda$ are shown in Fig. 8a, b, c. The values of λ considered here are those obtained taking into account the interference with the reflected rays, in all the cases where this interference is significant. By these fits we derive the nuclear interaction radii relative

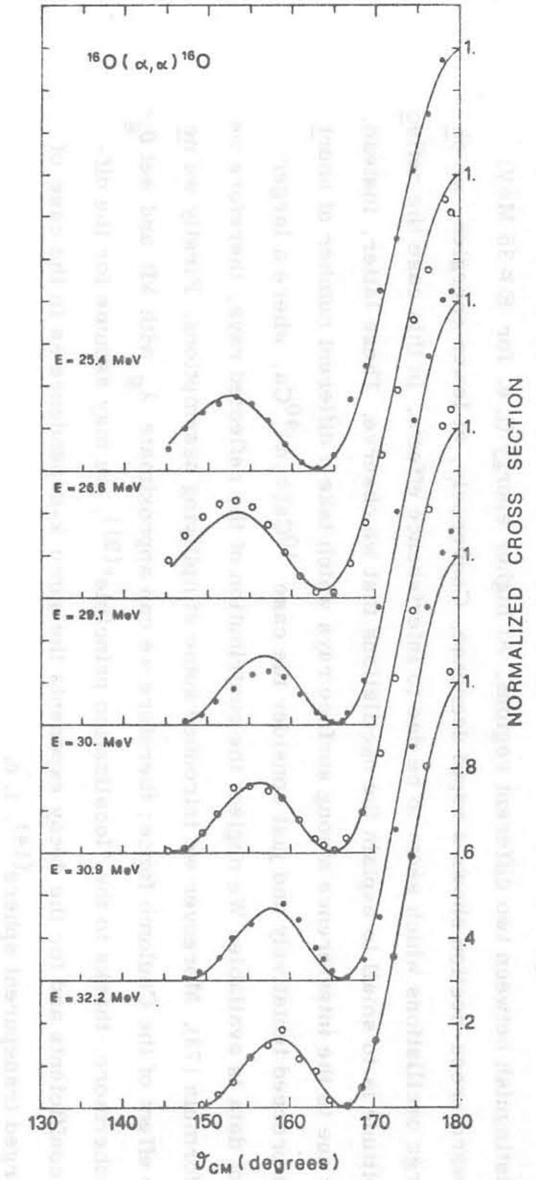

FIG. 7 - Fits to $^{16}O(\alpha,\alpha)^{16}O$ data from 25.4 to 32.2 MeV. The data are taken from ref. (8).

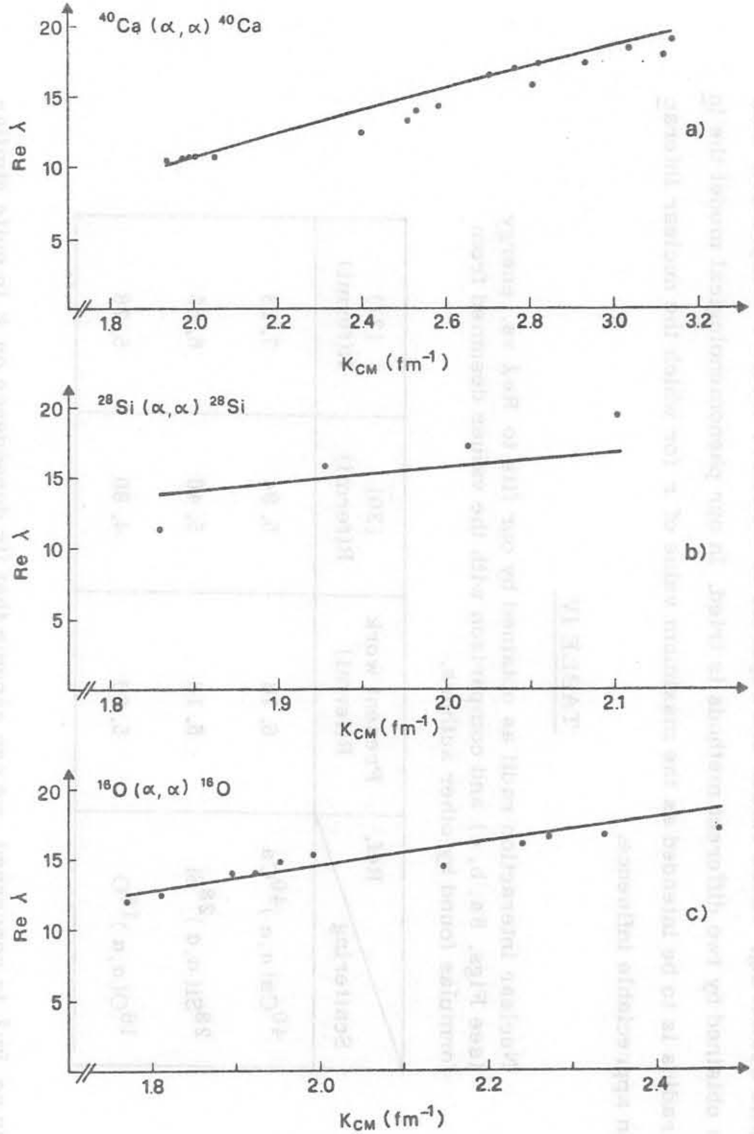

FIG. 8 - Fits of Reλ vs. incident wavenumber in the C. M. S. a) $^{40}Ca(\alpha,\alpha)^{40}Ca$; b) $^{28}Si(\alpha,\alpha)^{28}Si$; c) $^{16}O(\alpha,\alpha)^{16}O$. The values of Re$\lambda$ that we have used are desumed from the fit parameters at fixed energies (see Tables I, II and III). The results are reported in Table IV.

to the elastic scattering. These values are reported in Table IV, where a comparison with the values obtained by two different methods is tried. In our phenomenological model the interaction radius is to be intended as the maximum value of r for which the nuclear interaction has an appreciable influence.

TABLE IV

Nuclear interaction radii as obtained by our fits to $Re\lambda$ vs. energy (see Figs. 8a, b, c) and comparison with the values desumed from formulas found by other authors.

Scattering \ Ref.	Present work R(fermi)	(30) R(fermi)	(31) R(fermi)
$^{40}Ca(\alpha,\alpha)^{40}Ca$	6.76	5.94	7.13
$^{28}Si(\alpha,\alpha)^{28}Si$	6.16	5.46	6.55
$^{16}O(\alpha,\alpha)^{16}O$	5.30	4.80	5.78

As far as $Im\lambda$ is concerned, we can assume that its dependence on k is quite similar to the one that was calculated for an unchanged transparent sphere[14], i.e. that $Im\lambda$ increases slowly with energy. This is in qualitative agreement with the behaviour of the values that we have found (see Tables I, II, III). However, since the uncertainty in the determination of $Im\lambda$ is quite large, a precise fitting is, at the moment, meaningless.

Now let us consider the fits at fixed angle, i.e. at $\vartheta \simeq \pi$. Here the situation is much more involved and the experimental data are less precise. Also in this case it is convenient to distinguish between two different regions. At higher energy (i.e. for $E \gtrsim 35$ MeV) the backward cross-section shows a rapid decrease. Conversely, at lower energies, we observe large oscillations which seem to be due to interference effects. In this case the reflection amplitude is to small to explain the oscillations that we observe. These latter, instead, might be due to the interference among surface rays which take a different number of shortcuts. We proceed tentatively and just consider the case $^{40}Ca(\alpha,\alpha)^{40}Ca$, where a larger number of data is available. We neglect the contribution of the reflected rays, therefore we can use formula (73). Moreover we introduce some simplifying assumptions. Firstly we neglect the effect of the Coulomb force; therefore we can approximate λ_g with kR and set $\vartheta_g = 0$. Furthermore, thanks to the "localization principle"[21], we may assume for the diffraction coefficients and for the decay exponents the same k-dependence as in the case of an uncharged transparent sphere[14], i.e.

$$DD' = dk^{-1/6}, \tag{78}$$

$$\lambda = \lambda_g + i\alpha \simeq kR + (a + ib)k^{1/3} \tag{79}$$

where a and b are real positive constants, while d is a complex number. Lastly we just consider the contribution of the terms relative to p = 0, 1, 2 shortcuts. Then formula (73) becomes :

$$\left(\frac{d\sigma}{d\Omega}\right)_{\varphi=\pi} = k^{2/3} \; e^{-2\pi b k^{1/3}} \left| \sum_{p=0}^{2} L_p z^p \right|^2 \tag{80}$$

where

$$L_p = 2\pi R^3 \left| d \right|^2 \mathscr{L}_p(\nu_p) \tag{81}$$

and

$$z = e^{i(\Phi_s - \lambda\vartheta_t - \frac{\pi}{2})} \tag{82}$$

If, in addition, we neglect the term $ak^{1/3}$ in the expression of λ (as we did in the fits to the values of Reλ), and assume that Φ_s is proportional to k, formula (82) reads as follows:

$$z = e^{(b\vartheta_t k^{1/3} + i\varphi)} \tag{83}$$

where φ is a real function which depends linearly on k. Formula (80) has been used to fit the data up to $E \simeq 36$ MeV; the fit is shown in Fig. 9a. Here we do not make a best fit, but only a fit with the constraint that some of the parameters involved (e.g. ϑ_t) should assume reasonable values. The theoretical curve fits only qualitatively the experimental data, in the sense that it simply reproduces their oscillating trend. However, taking into account the crudeness of the model, such a discrepancy is not surprising.

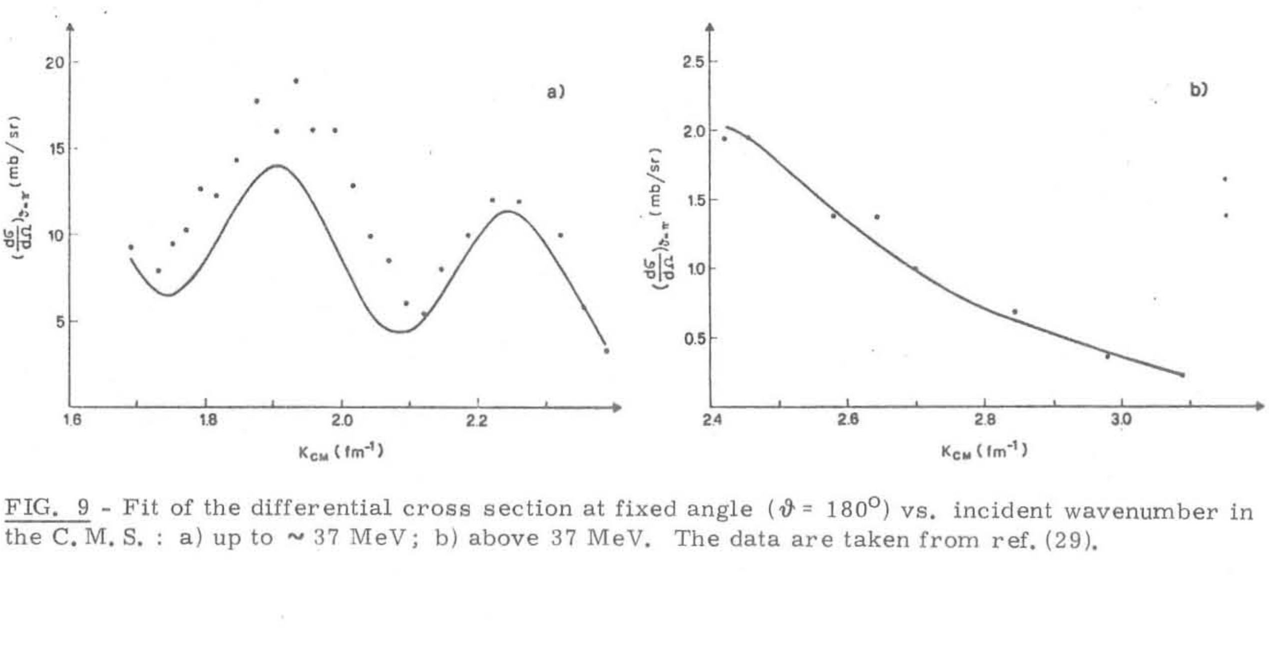

FIG. 9 - Fit of the differential cross section at fixed angle ($\vartheta = 180^o$) vs. incident wavenumber in the C.M.S. : a) up to ~ 37 MeV; b) above 37 MeV. The data are taken from ref. (29).

For higher energies we have to keep into account the effect of the expansion of the opacity region. As we have already said, this effect causes an attenuation of the amplitudes relative to the rays which take shortcuts. We take this effect into account by modifying formula (80) in a suitable way : we neglect the rays which take two shortcuts, i. e. we set $L_2 = 0$, and suppose that the amplitude relative to the rays with one shortcut is linearly decreasing with k. Finally formula (80), modified in this sense, is used to fit the data in the energy range from 36 to 65 MeV. The fit is shown in Fig. 9b.

In conclusion we can say that :

a) The role of the surface waves is evident in the energy range between $\sim$35 MeV and $\sim$60 MeV, especially in the case $^{40}Ca(\alpha,\alpha)^{40}Ca$.

b) At lower energies the physical situation is much more involved and interference mechanisms are necessary to explain the experimental data.

We have examined two possible types of interference.

i) Interference of the surface waves with the reflected rays ; this interference could be relevant for reproducing correctly the oscillations of the cross-sections at fixed energy.

ii) Interference of surface waves with a different number of shortcuts (different p); this mechanism could explain the large oscillations observed in the cross-section at fixed angle $(\vartheta - \pi)$ up to $\simeq$ 35 MeV.

ACKNOWLEDGEMENTS.

We are grateful to profs. R. Anni, L. Renna and U. Trevisan for useful and stimulating discussions. Moreover we are deeply indebted to all the authors who kindly sent us the numerical data used in the present paper : profs. A. Budzanowski, A. A. Cowley, A. G. Drentje, F. Michel, L. W. Put, J. Steyaert and W. T. H. Van Oers.

APPENDIX.

In this Appendix we treat the case of the grazing rays. In this connection it is convenient to analyse the trajectories in the following three regions separately: before the collision; on the sphere; after the collision. Then let us start to consider the first region.

a) Here we apply eq. (45) to an incident ray. We shall denote by Q and Q' two points of the ray considered, at distances r_o and r' respectively from the origin. Next the points Q and Q' shall be pushed up to infinity and up to the point Q_1 (see Fig. 10) respectively.

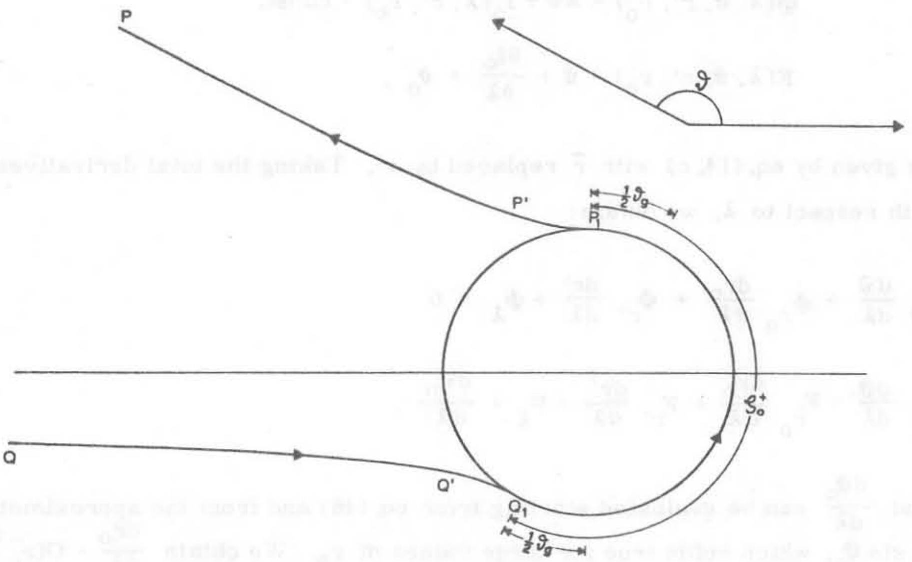

FIG. 10 - Diffracted ray in the direction ϑ: case p = 0, counterclockwise travelling wave.

Here and in the following we shall denote by $\overline{g}_Q$ the modulus of the fundamental vector product relative to the wavefront passing through Q, by $\overline{g}_{Q'}$ the same quantity relative to Q' and so on. Now, the value of $\overline{g}_Q$ can be deduced from eq. (47), setting $\lambda = \lambda_g$: we get

$$\overline{g}_Q = \frac{\lambda_g}{k}(1 + O(r_o^{-4})) . \tag{A.1}$$

Furthermore, if we parametrize the wavefront in Q' by ϑ and φ, $\overline{g}_{Q'}$ is given by:

$$\overline{g}_{Q'} = r'^2 \sin\vartheta \left[1 + \frac{1}{r'^2} \left(\frac{dr'}{d\vartheta}\right)^2_{\lambda=\lambda_g} \right]^{1/2} . \tag{A.2}$$

Besides we have to evaluate the Jacobian $\left|\frac{\partial(U,V)}{\partial(u,v)}\right|$ (see eq. (45)), which, in our case, reduces to $k\left|\frac{d\vartheta}{d\lambda}\right|_{\lambda=\lambda_g}$. In conclusion we have

$$k\bar{g}_{Q'}\left|\frac{d\vartheta}{d\lambda}\right|_{\lambda=\lambda_g} = kr'^2 \sin\vartheta\left[\left(\frac{d\vartheta}{d\lambda}\right)^2_{\lambda=\lambda_g} + \frac{1}{r'^2}\left(\frac{dr'}{d\lambda}\right)^2_{\lambda=\lambda_g}\right]^{1/2} \tag{A.3}$$

and we are faced with the problem of evaluating $\left(\frac{d\vartheta}{d\lambda}\right)_{\lambda=\lambda_g}$ and $\left(\frac{dr'}{d\lambda}\right)_{\lambda=\lambda_g}$ on the wavefront passing through Q'. We have at our disposal the equations of the wavefront and of the trajectory, i. e.

$$\Phi(\lambda, \vartheta, r', r_o) = \lambda\vartheta + I_o(\lambda, r', r_o) = \text{const.} \tag{A.4a}$$

$$F(\lambda, \vartheta, r', r_o) = \vartheta + \frac{\partial I_o}{\partial\lambda} = \vartheta_o \,, \tag{A.4b}$$

where I_o is given by eq. (14. c) with $\bar{r}$ replaced by r'. Taking the total derivatives of eqs. (A.4a, b) with respect to λ, we obtain:

$$\Phi_\vartheta \frac{d\vartheta}{d\lambda} + \Phi_{r_o}\frac{dr_o}{d\lambda} + \Phi_{r'}\frac{dr'}{d\lambda} + \Phi_\lambda = 0 \tag{A.5a}$$

$$F_\vartheta \frac{d\vartheta}{d\lambda} + F_{r_o}\frac{dr_o}{d\lambda} + F_{r'}\frac{dr'}{d\lambda} + F_\lambda = \frac{d\vartheta_o}{d\lambda} \,. \tag{A.5b}$$

But $\frac{dr_o}{d\lambda}$ and $\frac{d\vartheta_o}{d\lambda}$ can be evaluated starting from eq. (46) and from the approximate relation $\lambda \cong kr_o \sin\vartheta_o$, which holds true for large values of r_o. We obtain $\frac{dr_o}{d\lambda} = O(r_o^{-1})$ and $\frac{d\vartheta_o}{d\lambda} = O(r_o^{-1})$. On the other hand Φ_{r_o} and F_{r_o} remain finite for any finite value of r_o and also for $r_o \to \infty$. Therefore, when Q is pushed to infinity, the terms where $\frac{dr_o}{d\lambda}$ appears can be neglected and the eqs. (A.5a, b) can be regarded as a linear system to be solved with respect to $\frac{d\vartheta}{d\lambda}$ and to $\frac{dr'}{d\lambda}$. Moreover, pushing Q' to Q_1, we must set $r' = R$. The solution of our system is:

$$\left(\frac{d\vartheta}{d\lambda}\right)_{\substack{\lambda=\lambda_g \\ r'=R}} = O(r_o^{-1}) \tag{A.6a}$$

$$\left(\frac{dr'}{d\lambda}\right)_{\substack{\lambda=\lambda_g \\ r'=R}} = \frac{1}{k}\cos\left(\frac{\vartheta_s}{2}\right). \tag{A.6b}$$

Furthermore when Q' tends to Q_1, $\sin\vartheta$ becomes $\cos\left(\frac{\vartheta_g}{2}\right)$. Substituting all these quantities in formula (A.3) and using eq. (45) we get the following expression for the amplitude of the incident beam at Q_1, which shall be denoted by $A_i(Q_1)$:

$$A_i(Q_1) = \left[\frac{n(Q)}{n(Q_1)} \frac{\lambda_g}{kR} \frac{1}{\cos^2(\vartheta_g/2)}\right]^{1/2} \tag{A.7}$$

where $n(Q)$ and $n(Q_1)$ are the refractive index at Q and Q_1 respectively. The amplitude A_o at Q has been omitted, since it is set equal to 1 owing to the normalization constraint.

b) In this Appendix we shall speak of wavefunction and we shall use the symbol Ψ; indeed we are referring to the grazing trajectories only, and to their contribution to the wavefunction. Then the incident wavefunction at the point Q_1 has the following form : $A_i(Q_1)\exp\left[i\,\Delta_g\right]$, where $A_i(Q_1)$ and Δ_g are given by formulae (A.7) and (35) respectively. But at Q_1 we have the phenomenon of diffraction. Following Levy-Keller[2] we assume that the diffracted wavefunction is proportional to the incident one, through a proportionality factor depending on the incident wavefunction and on the local properties of the surface. This factor we define as $R^{1/2}D(Q_1)$, where $D(Q_1)$ is the (dimensionless) diffraction coefficient (see also ref. (14)). Thus, assuming that the phases of the incident and the diffracted wavefunctions are equal[2], and denoting the diffracted wavefunction by $\psi_d(Q_1)$, we have :

$$\psi_d(Q_1) = R^{1/2} D(Q_1) A_i(Q_1)\, e^{i\Delta_g} . \tag{A.8}$$

Let us consider, for the moment, only those rays which do not undergo any shortcuts (p = 0). The surface ray starts at Q_1, then it describes a tract of geodesic along the surface of the interaction region. At each point the ray splits, one part continuing along the surface and the other part leaving the surface along the tangent to the geodesic. Thus at the point P_1 (see Fig. 10) the phase is given by :

$$\Phi_d(P_1) = \Phi_d(Q_1) + {}_cR\,\zeta_o^+ = \Delta_g + k_c R\,\zeta_o^+ , \tag{A.9}$$

where ζ_o^+ is the arc described by the surface ray. Furthermore we introduce a decay exponent α, which describes the decay due to the ray splitting exposed above. In conclusion the wavefunction in P_1 is given by[2] :

$$\psi_d(P_1) = \left(\frac{d\sigma_o}{d\sigma}\right)^{1/2} e^{-\alpha\,\zeta_o^+}\, e^{ik_c R\,\zeta_o^+}\, \psi_d(Q_1) \tag{A.10}$$

where $d\sigma_o/d\sigma$ is the ratio of the strip width of surface rays at Q_1 to that at P_1. A simple geometric calculation gives :

$$\frac{d\sigma_o}{d\sigma} = \frac{\cos\left(\frac{\vartheta_g}{2}\right)}{\cos\left(\zeta_o^+ - \frac{\vartheta_g}{2}\right)} . \tag{A.11}$$

Finally in formula (A.10) the product of the exponentials $\exp(-\alpha\zeta_o^+)$ and $\exp(i k_c R\, \zeta_o^+)$ can be rewritten as follows: $\exp i\left[(k_c R + i\alpha)\,\zeta_o^+\right]$; thus we introduce a complex valued angular momentum: $\lambda = k_c R + i\alpha$.

c) From the point P_1 the tangent ray travels to P at a distance r from the origin (see Fig.10). Let P' denote a point on the diffracted ray from P_1 to P, at a distance r' from the origin. We can apply once more eq. (45) in the tract P'P; then we shall push P' to P_1 and P to infinity. Therefore we must evaluate $\bar{g}_{P'}$ and $\bar{g}_P$. If we parametrize the diffracted wavefronts in P and in P' by ϑ and φ we obtain formulas similar to (A.2). So we are faced with the problem of deducing the expressions of $dr/d\vartheta$ and $dr'/d\vartheta$ on the wavefronts passing through P and P'. To this end we write the phase of the diffracted rays, from the point of incidence Q_1 to a generical point on the diffracted ray (say P), as the sum of two addends: the phase difference Φ_s between Q_1 and P_1, along the geodesic, and the phase Φ_t of P relative to P_1 along the diffracted ray, tangent to the surface. So we have:

$$\Phi_s = \lambda_g\, \zeta_o^+ \tag{A.12}$$

$$\Phi_t = \lambda_g\left[\vartheta - \left(\frac{\pi}{2} + \zeta_o^+ - \frac{\vartheta_g}{2}\right)\right] + I(\lambda_g, R, r) \tag{A.13}$$

where $I(\lambda_g, R, r)$ is given by eq. (14.b) with R in place of $\bar{r}$ and λ_g instead of λ. Next we write the equation of the wavefront of the diffracted rays as follows:

$$\Phi_s + \Phi_t = \lambda_g\left(\vartheta + \frac{\vartheta_g}{2} - \frac{\pi}{2}\right) + I(\lambda_g, R, r) = \text{const.} \tag{A.14}$$

Deriving (A.14) with respect to ϑ, we get:

$$\lambda_g + \frac{dI}{dr}\,\frac{dr}{d\vartheta} = 0 \tag{A.15}$$

whence we derive the expression of $dr/d\vartheta$. We can proceed analogously for obtaining $dr'/d\vartheta$. Substituting these quantities in eq. (A.2) we get:

$$\bar{g}_{P'} = r'^2\left|\sin\vartheta\right|\left(\frac{k^2 r'^2 - 2\eta k r'}{k^2 r'^2 - 2\eta k r' - \lambda_g^2}\right)^{1/2} \tag{A.16}$$

and

$$\bar{g}_P = r^2\left|\sin\Theta\right|\left(1 + O(r^{-2})\right) \tag{A.17}$$

where, as usual, the deflection angle Θ is given by:

$$\Theta = \lim_{r \to \infty} \vartheta(r) = \pi - \vartheta_g + \zeta_o^+ \; . \tag{A.18}$$

The Jacobian $\left| \dfrac{\partial(U,V)}{\partial(u,v)} \right|$ (see eq. (45)) reduces to $\left| \dfrac{d\vartheta}{d\Theta} \right|$. To evaluate this derivative, let us write the equation of the trajectory of the diffracted ray :

$$\vartheta(r) = \frac{\pi}{2} - \frac{\vartheta_g}{2} + \zeta_o^+ + \int_R^r \frac{\lambda_g \, dr'}{r'(k^2 r'^2 - 2\eta k r' - \lambda_g^2)^{1/2}} \; . \tag{A.19}$$

From this equation we derive ζ_o^+ in terms of $\vartheta(r)$; next substituting this expression of ζ_o^+ in eq. (A.18) and taking the total derivative of Θ with respect to ϑ we get :

$$\frac{d\Theta}{d\vartheta} = \frac{k^2 r'^2 - 2\eta k r'}{k^2 r'^2 - 2\eta k r' - \lambda_g^2} \; . \tag{A.20}$$

Putting (A.16), (A.17) and (A.20) in eq. (45) and neglecting terms of order $O(r^{-2})$, we get :

$$\left[A_f(P')\right]^2 n(P') r'^2 \left|\sin\vartheta\right| \left(\frac{k^2 r'^2 - 2\eta k r' - \lambda_g^2}{k^2 r'^2 - 2\eta k r'} \right)^{1/2} = \left[A_f(P)\right]^2 n(P) r^2 \left|\sin\Theta\right| \tag{A.21}$$

where A_f denotes the amplitude of the outgoing wave. In this case, however, we are faced with a difficulty in doing the limit for $P' \to P_1$. Indeed the surface of the obstacle is a caustic of the diffracted rays ; then the amplitude becomes infinite, at least within the approximation of geometrical ray tracing. But observe that the term $(k^2 r'^2 - 2\eta k r' - \lambda_g^2)^{1/2}$ goes to zero as $r' \to R$. Then, in analogy with a procedure followed by Levy-Keller[2], we introduce the following quantity :

$$\left[A(P_1)\right]^2 = \lim_{r' \to R} \left[A_f(P')\right]^2 \left(r'^2 - \frac{2\eta r'}{k} - \frac{\lambda_g^2}{k^2}\right)^{1/2} \tag{A.22}$$

which is certainly finite thanks to the eq. (A.21). Furthermore observing that $\sin\vartheta$ becomes $\cos\left(\zeta_o^+ - \dfrac{\vartheta_g}{2}\right)$ as $P' \to P_1$, from eqs. (A.21) and (A.22) we get :

$$A_f(P) = R \, \frac{A(P_1)}{r\left|\sin\Theta\right|^{1/2}} \left[\frac{k}{\lambda_g} \cos\left(\zeta_o^+ - \frac{\vartheta_g}{2}\right) \frac{n(P_1)}{n(P)} \right]^{1/2} . \tag{A.23}$$

now we can assume, in analogy with the procedure followed by Levy-Keller[2], that $A(P_1)$ is proportional to the amplitude of the diffracted wavefunction $\psi(P_1)$, through a dimensionless proportionality coefficient $D'(P_1)$. Then, owing to the reciprocity principle[2], we can regard this factor as a diffraction coefficient; moreover, thanks to the spherical symmetry of the obstacle, we can say that $D'(P_1) = D(Q_1)$. However, since we are interested to making a phenomenological extension of the model (see section 3), where this equality may be no longer true, we prefer to indicate the two diffraction coefficients by two different symbols. Concerning the phase of the outgoing wave at the point P_1, it is assumed equal to the phase of the surface ray at the same point, i.e. $\Delta_g + k_c R\,\zeta_o^+$ (see formula (A.9)). Then the wavefunction at the point P_1 is given by:

$$\psi_f(P_1) = D'(P_1)\,\psi_d(P_1)\,. \tag{A.24}$$

Furthermore the wavefunction at the point P shall be given by : $A_f(P)\exp\left[i\Phi_f\right]$, where $A_f(P)$ is given by formula (A.23) and Φ_f is given by:

$$\Phi_f = 2\,\Delta_g + kr - \eta\log 2kr + k_c R\,\zeta_o^+\,. \tag{A.25}$$

Collecting all the results we finally obtain:

$$\psi_f(P) = R\,\frac{D(Q_1)\,e^{i\lambda\zeta_o^+}\,e^{2i\eta\left[\log(kR-\eta)-1\right]}\,D'(P_1)}{(\sin\vartheta)^{1/2}\,(\cos\frac{\vartheta_g}{2})^{1/2}}\;\frac{e^{i\left[kr-\eta\log 2kr\right]}}{r} \tag{A.26}$$

where $\lambda = k_c R + i\alpha$, and in place of Δ_g we have written its expression given by formula (35). Furthermore we have used, in formula (A.26), the scattering angle ϑ instead of the deflection angle Θ. In this connection let us deduce the general relationship between the deflection angle Θ and the scattering angle ϑ for the diffracted rays. We have:

$$\Theta = \pi - \vartheta_g + \zeta_p^{\pm} + p\vartheta_t + 2m\pi \qquad (m = 0,1,2,\dots) \tag{A.27}$$

where $\zeta_o^{\pm}$ are defined by formula (52.b). This latter formula can be rewritten in the following way:

$$\zeta_p^{\pm} = \vartheta_g - p\vartheta_t \pm \vartheta + 2n\pi \tag{A.28}$$

where n is such that $0 \le \zeta_p^{\pm} \le 2\pi$. Therefore substituting (A.28) in (A.27) we obtain:

$$\Theta = \pm\vartheta + \left[2(m+n)+1\right]\pi\,. \tag{A.29}$$

Let us remark that if the surface ray is critically refracted at a point S_1, takes a shortcut S_1S_2 and reemerges at S_2 (see Fig. 11), then we can repeat arguments quite close to those developed before.

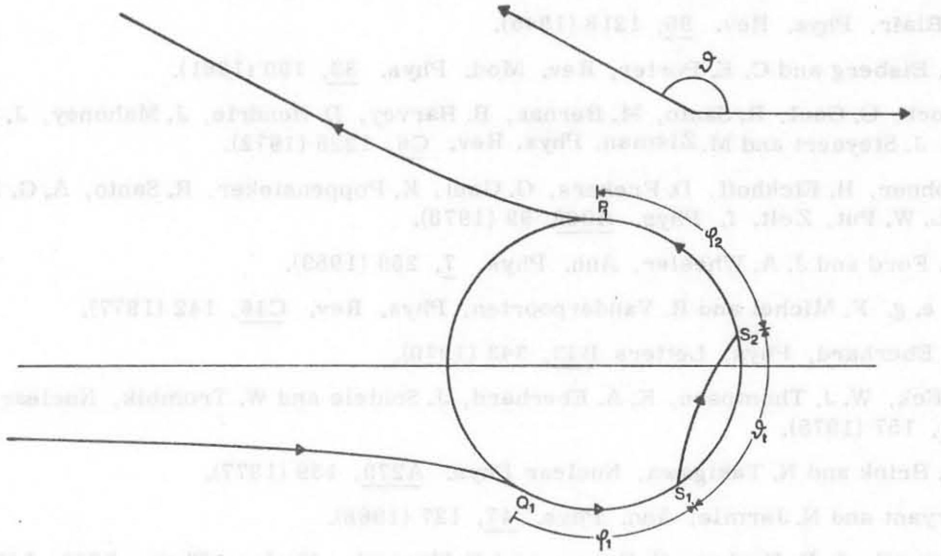

FIG. 11 - Diffracted ray in the direction ϑ : case p = 1, counterclockwise travelling wave. One has $\zeta_1^+ = \varphi_1 + \varphi_2$. (The shortcut is represented only qualitatively).

In particular we can apply eq. (45) to the shortcut S_1S_2 and use the symmetry of the trajectory with resoect to the point of minimal distance. The result is :

$$\Psi_f(P) = R \, \frac{D e^{i\lambda\zeta_1^+} D_{12} \, e^{i\Phi_s} D_{21} D' \, e^{2i\eta\left[\log(kR-\eta)-1\right]}}{(\sin\vartheta)^{1/2} \, (\cos\frac{\vartheta_g}{2})^{1/2}} \; \frac{e^{i\left[kr - \eta\log 2kr\right]}}{r} \qquad \text{(A.30)}$$

where D_{12} and D_{21} are coefficients of proportionality for the rays which enter into or emerge from the sphere; $\exp(i\Phi_s)$ is the propagator for the shortcut and it is given explicitly by formula (54); lastly the scattering angle ϑ is related to ζ_1^+ through formula (A.28) setting p = 1.

REFERENCES

(1) - J. B. Keller, Proc. Symp. Applied Mathematics 8, 27 (1958).

(2) - B. R. Levy and J. B. Keller, Comm. Pure Appl. Math. 12, 159 (1959).

(3) - J. S. Blair, Phys. Rev. 95, 1218 (1945).

(4) - R. M. Eisberg and C. E. Porter, Rev. Mod. Phys. 33, 190 (1961).

(5) - R. Stock, G. Gaul, R. Santo, M. Bernas, B. Harvey, D. Hendrie, J. Mahoney, J. Sherman, J. Steyaert and M. Zisman, Phys. Rev. C6, 1226 (1972).

(6) - H. Lohner, H. Eickhoff, D. Frekers, G. Gaul, K. Poppensieker, R. Santo, A. G. Drentje and L. W. Put, Zeit. f. Phys. A286, 99 (1978).

(7) - K. W. Ford and J. A. Wheeler, Ann. Phys. 7, 259 (1959).

(8) - See, e. g. F. Michel and R. Vanderpoorten, Phys. Rev. C16, 142 (1977).

(9) - K. A. Eberhard, Phys. Letters B33, 343 (1970).

(10) - J. S. Eck, W. J. Thompson, K. A. Eberhard, J. Schiele and W. Trombik, Nuclear Phys. A255, 157 (1975).

(11) - D. M. Brink and N. Takigawa, Nuclear Phys. A279, 159 (1977).

(12) - H. Bryant and N. Jarmie, Ann. Phys. 47, 127 (1968).

(13) - H. Uberall, A. R. Farhan, O. Dragun and E. Maqueda, Nuclear Phys. A362, 241 (1981).

(14) - H. M. Nussenzveig, Journ. Math. Phys. 10, 82 and 125 (1969).

(15) - E. Di Salvo and G. A. Viano, Nuovo Cimento B33, 547 (1976).

(16) - J. Hadamard, Lectures on Cauchy's Problem in Linear Partial Differential Equations, (New York, 1952).

(17) - H. Goldstein, Classical Mechanics (Massachusetts, 1965), Chap. 9.

(18) - L. Landau and E. Lifchitz, Mécanique Quantique (Moscow, 1966), p. 151.

(19) - R. Anni, L. Renna and L. Taffara, Nuovo Cimento A55, 456 (1980).

(20) - Y. M. Chen, Journ. Math. Phys. 5, 820 (1964).

(21) - E. Di Salvo and G. A. Viano, Nuovo Cimento A59, 11 (1980).

(22) - See ref. (6), Fig. 2.

(23) - Th. Delbar, Gh. Grégoire, G. Paic, R. Ceuleneer, F. Michel, R. Vanderpoorten, A. Budzanowski, L. Friendl, K. Grotowski, S. Micek, R. Planeta, A. Strzalkowski and K. A. Eberhard, Phys. Rev. C18, 1237 (1978).

(24) - W. T. H. Van Oers, G. J. C. Van Niftrik, H. L. Jonkers and K. W. Brockman Jr., Nuclear Phys. 74, 469 (1965).

(25) - J. Steyaert, private communication, unpublished data at Saclay, April 1966.

(26) - A. Budzanowski, K. Grotowski, L. Jarczyk, B. Lazarska, S. Micek, H. Nievodniczanski, A. Strzalkowski and Z. Wrobel, Phys. Letters 16, 135 (1965).

(27) - A. G. Drentje and J. D. A. Roeders, Kernfysisch Versneller Institut, Internal Report KVI-36, Rijksuniversiteit te Groningen, 1972 (unpublished).

(28) - A. A. Cowley and G. Heymann, Nuclear Phys. A146, 465 (1970).

(29) - See ref. (8), Fig. 6.

(30) - G. Igo, H. E. Wagner and R. Eisberg, Phys. Rev. 101, 1508 (1956).

(31) - See ref. (4), pag. 198

(32) - J. Lega and P. C. Macq, Nuclear Phys. A218, 429 (1974).